

# Efficient Parallel Data Optimization for Homogeneous Diffusion Inpainting of 4K Images \*

Niklas Kämper <sup>†</sup>, Vassillen Chizhov<sup>†</sup>, and Joachim Weickert<sup>†</sup>

**Abstract.** Homogeneous diffusion inpainting can reconstruct missing image areas with high quality from a sparse subset of known pixels, provided that their location as well as their gray or color values are well optimized. This property is exploited in inpainting-based image compression, which is a promising alternative to classical transform-based codecs such as JPEG and JPEG2000. However, optimizing the inpainting data is a challenging task. Current approaches are either fairly slow or do not produce high quality results. As a remedy we propose fast spatial and tonal optimization algorithms for homogeneous diffusion inpainting that efficiently utilize GPU parallelism, with a careful adaptation of some of the most successful numerical concepts. We propose a densification strategy using ideas from error-map dithering combined with a Delaunay triangulation for the spatial optimization. For the tonal optimization we design a domain decomposition solver that solves the corresponding normal equations in a matrix-free fashion and supplement it with a Voronoi-based initialization strategy. With our proposed methods we are able to generate high quality inpainting masks for homogeneous diffusion and optimized tonal values in a runtime that outperforms prior state-of-the-art by a wide margin.

**Key words.** Inpainting, Homogeneous Diffusion, Data Optimization, Domain Decomposition, GPU

**MSC codes.** 65N55, 65D18, 68U10, 94A08

**1. Introduction.** Inpainting-based image compression methods [1, 7, 19, 25, 32, 34, 47, 52, 62, 67, 70, 73, 84, 85, 86, 35] can be promising alternatives to classical transform-based codecs. During encoding, they store a small subset of pixels. In the decoding phase, the missing parts of the image are reconstructed from the stored pixels by an inpainting operator. Earlier approaches [1, 7, 19, 25, 34, 52, 86] mostly rely on image data at semantic image features such as edge locations. Many later approaches [32, 42, 62, 70] instead carefully optimize the locations of the known data, without any restrictions to semantic image features. In terms of quality, inpainting-based compression methods have been shown to be able to outperform the widely used JPEG [59] and JPEG2000 [77] for images with small to medium amounts of texture [62, 70].

Surprisingly, already with simple linear homogeneous diffusion [44] one can obtain very good inpainting results [8, 13, 16, 20, 39, 54] under the condition that the inpainting data are highly optimized. For piecewise constant images, such as cartoon images, depth maps or flow fields, one can even achieve state-of-the-art results [34, 42, 51, 53] and outperform HEVC [76]. In contrast to nonlinear inpainting methods, homogeneous diffusion inpainting is parameter-free and its discretization yields a sparse system that benefits from its linearity.

\*

**Funding:** This work has received funding from the European Research Council (ERC) under the European Union's Horizon 2020 research and innovation programme (grant agreement no. 741215, ERC Advanced Grant INCOVID)

<sup>†</sup>Mathematical Image Analysis Group, Faculty of Mathematics and Computer Science, Saarland University, 66041 Saarbrücken, Germany ([kaemper@mia.uni-saarland.de](mailto:kaemper@mia.uni-saarland.de), [chizhov@mia.uni-saarland.de](mailto:chizhov@mia.uni-saarland.de), [weickert@mia.uni-saarland.de](mailto:weickert@mia.uni-saarland.de))

In [49] it has been shown that we can solve this linear system in real-time for 4K color images.

Achieving good reconstruction quality with homogeneous diffusion inpainting requires, however, a careful optimization of the inpainting data that we store in the encoding phase. This consists of selecting the subset of pixels to be stored (i.e. *the inpainting mask*) and optimizing the gray or color values at the stored pixels (i.e. *the tonal data*). Usually, these optimizations are computationally much more expensive than the inpainting itself, and even though the encoding phase often does not have to be performed in real-time, it is still desirable to have highly efficient methods.

Most approaches for spatial optimization either focus on high quality masks [20, 39, 54] at a high computational cost, or lower quality masks [8] at a much lower cost. In practice one typically does not aim at either extreme, and we are instead interested in methods that can achieve good quality in reasonable time [21, 23, 50, 71]. Our GPU-based implementation in the present work is orders of magnitude faster than the spatial optimization in [21, 23, 50], which makes it a practical approach for mask optimization of 4K images. A GPU-based algorithm also targeted at 4K spatial optimization, and comparable in terms of efficiency, is the recent neural approach by Schrader et al. [71]. We outperform the latter in terms of quality and speed, while having much lower memory requirements.

For the tonal optimization problem all methods can theoretically achieve the same reconstruction quality, as it is a linear least squares problem with a unique solution for non-empty masks [53], and thus there are no risks of getting stuck in local minima. Approaches based on inpainting echoes [54] or Green’s functions [41] are unsuitable for large images due to the memory constraints imposed by the arising dense systems, or the large computational cost of their matrix-free variants. For this reason we do not discuss them in this paper beyond a short overview of the literature. Other viable alternatives include [20, 40, 41, 54, 64], however, all of those are orders of magnitude slower than our proposed GPU-based algorithm. Even the recent approach by Chizhov and Weickert [21], which is one of the fastest on masks of 5% density, takes approximately 10 minutes for the tonal optimization of a 4K color image. While these methods can be improved with parallel GPU implementations, and we do implement several of those on the GPU for comparison, they are still not able to reach the efficiency of our method, which is specifically designed for highly parallel architectures such as GPUs.

**1.1. Our Contribution.** The goal of our paper is to develop a state-of-the-art data optimization framework for homogeneous diffusion inpainting that complements the fast inpainting solver from [49]. To this end, we devise fast and highly parallel methods to optimize the data to be stored. This allows us to construct the first viable data optimization approach for sparse 4K image inpainting in high quality that also exploits tonal optimization.

For the spatial optimization we extend the densification approaches by Daropoulos et al. [23], and Chizhov and Weickert [21]. We employ a Delaunay-based densification, which we supplement with a strategy for choosing the initial inpainting mask, based on the analytic mask optimization framework of Belhachmi et al. [8]. Our methods offer state-of-the-art performance. We achieve fast runtimes by efficiently computing the Delaunay triangulation in each densification iteration from an approximation of the Voronoi tessellation, obtained with the *jump flood algorithm (JFA)* [68].

For our tonal optimization approach, inspired by the nested *conjugate gradients (CG)*

approach by Chizhov and Weickert [21], we solve the corresponding normal equations in a matrix-free fashion. Instead of relying on CG, we construct a novel highly parallel solver for tonal optimization adapted to our sparse inpainting problem. It carefully adapts and integrates ideas from multigrid and domain decomposition, see Figure 6. As an outer solver, we adapt a *restricted additive Schwarz* domain decomposition method [18], which is able to exploit the fact that the influence area of each known pixel is localized in practice. In addition, we devise a computationally inexpensive initialization strategy allowing for a much earlier termination of the tonal optimization. We derive the latter from a theoretically motivated surrogate problem, which also subsumes the initialization from the work of Galić et al. [32].

Since our spatial and tonal optimization methods both require the computation of multiple inpainting solutions, we use the multigrid ORAS inpainting solver proposed in [49]. This is to the best of our knowledge the fastest homogeneous diffusion inpainting solver for parallel architectures such as GPUs. Thanks to all of our contributions, we are able to achieve runtimes of less than a second for the full data optimization of 4K color images with an optimal linear scaling behavior with respect to the image resolution. Our tonal optimization is currently the fastest method for homogeneous diffusion inpainting, taking less than half a second for a 4K RGB image. Our spatial optimization is the second fastest available mask optimization approach, also taking less than half a second for the construction of outstanding quality masks for a 4K RGB image. The only faster spatial optimization strategy is the method by Belhachmi et al. [8], however, it results in inpaintings that can have a PSNR of up to 6 dB lower compared to our approach, see Figure 10.

**1.2. Related Work.** In the following we discuss prior works on spatial and tonal optimization and how they are related to our framework.

**1.2.1. Spatial Optimization.** Finding a subset of pixels to be stored that result in a high quality reconstruction is a challenging combinatorial optimization problem. Here we only focus on approaches for homogeneous diffusion-based inpainting in 2D. There are also a number of related works, for example the free knot problem for spline interpolation [72].

*Analytic Approach.* Belhachmi et al. [8] developed a framework for mask optimization based on a continuous shape analytic perspective of homogeneous diffusion inpainting, which was later extended by Belhachmi and Jacumin [10, 11] for noisy images. The practically relevant result is that the mask density should be chosen as an increasing function in the absolute value of the Laplacian of the target image. In the discrete setting they suggest applying a dithering method to the absolute value of the smoothed Laplacian image, e.g. Floyd-Steinberg dithering [31], in order to generate a mask that matches the desired density. While this approach is very fast, as it does not require computing any inpaintings, in practice the dithering approximation leads to a limited reconstruction quality [54]. In the current work we aim at a considerably higher quality of the inpaintings, and therefore integrate the Belhachmi approach only as a partial initialization in our algorithm.

*Gradient-based Methods.* With non-smooth optimization strategies such as primal-dual solvers and optimal control, one can obtain high-quality non-binary inpainting masks [13, 20, 39, 57]. For compression purposes, however, the masks have to be binarized, which reduces the quality [40]. Nevertheless, these methods produce state-of-the-art masks but have a prohibitively large runtime even for small images. Since we aim at fast algorithms that scale to 4K

images, we instead consider greedier strategies that produce good results in short runtimes.

*Sparsification.* Mainberger et al. [54] have proposed a *probabilistic sparsification (PS)* algorithm that starts with a full mask and iteratively removes pixels from the mask until the desired density is reached. In each iteration, a set of candidate pixels from the mask is chosen and temporarily removed. An error map is computed from the inpainting with the reduced mask. Then a fixed number of the candidates are reintroduced back into the image: the ones with the highest pointwise errors. While this approach can be easily adapted to different inpainting operators, such as PDE-based ones [54] or linear splines interpolation over triangulations [24], it is computationally fairly expensive. Additionally, since PS starts from a full mask, reaching low densities takes many more iterations than starting from an empty mask and densifying. Last but not least, PS is prone to getting stuck in suboptimal local minima both because it uses only pointwise errors as an oracle, and because the error itself in the initial iterations is a result only of a very localized neighborhood that is not predictive of the influence of mask points in later iterations. These considerations suggest studying densification approaches with an oracle that adapts to the density of the mask in each iteration.

*Densification.* Densification approaches start from an empty mask and iteratively insert new pixels. In practice, this also means that fewer iterations need to be performed compared to sparsification-based methods, since the usual mask densities for inpainting-based compression are below 10%. In compression settings, densification has been successfully applied to constrained data structures such as subdivision trees [27, 32, 62, 70]. In the current work we are interested in the more general case of unconstrained masks. Unconstrained densification strategies have been used successfully for diffusion-based [9, 21, 23, 45, 80] and exemplar-based [50] inpainting, as well as as linear interpolation on Delaunay triangulations [3, 30]. The works of Daropoulos et al. [23], Chizhov and Weickert [21], and Jost et al. [45] consider not just pixel-wise errors, but aggregate the error over mask-adaptive neighborhoods based on the Voronoi diagram [23, 45] or the Delaunay triangulation [21], which improves the reconstruction quality compared to a pixel-wise densification. The work by Jost et al. [45] even generalizes the optimization to masks prescribing derivatives and local integrals. Currently, Voronoi- and Delaunay-based densification approaches provide the best quality-to-runtime ratio for mask construction, so we use those as a basis for the mask generation algorithms we develop in the present work.

*Non-local Pixel Exchange.* Even though densification-based methods can perform better than sparsification-based ones, they are still greedy and can thus get stuck in local minima. To alleviate this, a global relocation strategy called *nonlocal pixel exchange (NLPE)* has been devised by Mainberger et al. [54]. It stochastically chooses a mask pixel and a subset of non-mask pixels with high pointwise errors, and iteratively computes the errors for the reconstructions resulting from relocating the mask pixels to the candidate non-mask pixel locations. The best swap (potentially none) is kept. While this approach can escape from local minima and achieve significant improvements, it requires a huge number of iterations (i.e. computational resources) to converge. We also note that for linear spline interpolation on triangulations a similar approach has been used to optimize masks [55].

*Neural-based Approaches.* Besides model-based spatial optimization algorithms, a number of neural mask generation frameworks have been proposed in recent years. Dai et al. [22] developed a deep learning method for adaptive sampling that uses an inpainting network and

a mask optimization network, which are trained separately. In order to improve the quality, Peter [61] jointly trains inpainting and spatial optimization with Wasserstein GANs. Alt et al. [4] train a mask generator specifically for homogeneous diffusion inpainting. In order to be able to perform a fast backpropagation for the mask network they propose to replace the inpainting with a learned surrogate solver that approximates homogeneous diffusion inpainting, which is learned together with the mask network in a joint fashion. The efficiency has been improved further by Peter et al. [64] with a modified network architecture. The aforementioned networks were, however, only trained on small images which leads to a poor performance for 4K images. Due to memory and computational constraints, directly training on 4K images is infeasible on standard hardware.

To scale neural methods to 4K images, Schrader et al. [71] proposed a coarse-to-fine approach that divides the input image into small patches and creates an inpainting mask for each patch with a mask generation network. Each patch uses a mask density estimated by the average Laplacian magnitude according to the analytic approach by Belhachmi et al. [8]. This allows efficient scaling of the mask construction to higher resolutions, and is able to generate masks for 4K color images in less than 0.5 seconds on a high-end GPU.

While neural approaches have the advantage of not needing to perform several inpainting steps, model-based optimization is transparent, and the ideas within generalize to a larger class of problems. Therefore, in the current work we rely on non-neural optimization techniques. Thanks to using the fast inpainting solver, proposed in [49], and the efficient optimization algorithms developed in the current work, we are even able to achieve similar runtimes to the method by Schrader et al. [71] with much lower memory usage, while producing higher quality masks.

*Video Coding.* Most approaches for inpainting-based video compression, such as [5, 63], optimize the inpainting masks for each frame independently. Breuß et al. [16] instead optimize inpainting masks only for key frames, with the optimal control approach of Hoeltgen et al. [39]. For the intermediate frames, they use optical flow to interpolate the masks.

**1.2.2. Tonal Optimization.** After generating a mask, e.g. using one of the above algorithms, one can improve the reconstruction quality further by modifying the stored color values at mask pixels. This is done by minimizing some error metric with respect to the reference image. The mean squared error (MSE) is an especially appealing choice, since the global optimum of the optimization problem can be found by solving a linear system of equations (the normal equations). Consequently, we focus on methods that minimize the MSE.

*Matrix Structure.* The system matrix for the normal equations is of the form  $\mathbf{B}^\top \mathbf{B} \in \mathbb{R}^{m \times m}$ , where  $m$  is the number of mask pixels [41, 54]. The latter is a symmetric positive definite matrix. Such matrices are advantageous from a numerical perspective, since algorithms such as the Cholesky decomposition [38] or the conjugate gradient (CG) method [37, 69] can be used to efficiently compute a solution. We note, however, that neither  $\mathbf{B}^\top \mathbf{B}$  nor  $\mathbf{B}$  are sparse. Despite this, the matrix-vector product  $\mathbf{B}\mathbf{x}$  can be carried out through a sparse matrix-vector product followed by solving a sparse linear system, both of which can be implemented in a matrix-free fashion (i.e. without explicitly forming or storing the matrices).

*Direct vs Iterative Methods.* Linear system solvers can generally be split in two classes: direct ones and iterative ones. Classical direct methods, such as Cholesky, LU, or QR factor-

izations [38], are suited for dense and not too large matrices, and their runtime is typically independent of the condition number of the matrix (the latter can affect the numerical stability, however). Iterative solvers, such as CG [37, 69], on the other hand, scale favorably to large sparse problems and allow one to stop early, but their convergence speed is typically dependent on the condition number. In practice a matrix-free matrix-vector product can be integrated easily in iterative methods, and they are more readily parallelizable.

In our target case of tonal optimization for 4K images, a standard mask density of 5% results in a system matrix of size  $m \times m$  where  $m \approx 400000$ . As this matrix is dense, we would need approximately 640 GB of memory if we wished to form it and store it. On the other hand, as discussed, the product  $\mathbf{B}\mathbf{x}$  can be implemented in a matrix-free fashion. In practice, this constrains us to iterative approaches, but we nevertheless discuss some tonal optimization frameworks based on direct methods, since e.g. they have been shown to be able to outperform iterative approaches on masks with few pixels [41].

*Inpainting Echoes.* For smaller images one can compute the matrix  $\mathbf{B}$  explicitly and store it. The columns in this matrix are termed *inpainting echoes* [54]. Mainberger et al. [54] precompute the echoes and store them, and thus essentially form and store the matrix  $\mathbf{B}$ . They note that one could solve the normal equations involving  $\mathbf{B}^\top \mathbf{B}$  with an LU solver [38], but that this is too slow even for  $256 \times 256$  images. This supports our statement that for large images an iterative solver has to be used. They employ a modified successive over-relaxation (SOR) solver [69] with an under-relaxation weight and random mask points traversal. In practice, storing  $\mathbf{B}$  is infeasible for larger images due to memory constraints, and recomputing an inpainting echo (i.e. a column of  $\mathbf{B}$ ) each time a mask value needs to be modified in an iterative approach is also prohibitively expensive. In our method, we use a much more efficient way to evaluate products  $\mathbf{B}\mathbf{x}$  without ever explicitly forming or storing any matrix.

*Green's Functions.* Homogeneous diffusion inpainting can equivalently be formulated in terms of a linear combination of Green's functions associated with mask points [41, 43, 48]. The Green's functions are a kind of spectral counterpart to the inpainting echoes. We will denote the matrix of the Green's functions, for a specific mask, with  $\mathbf{G}$ . Then the corresponding normal equations take the form  $\mathbf{G}^\top \mathbf{G}$  once again [41]. The main difference to the inpainting echoes is that products  $\mathbf{G}\mathbf{x}$  can be evaluated efficiently and in a matrix-free fashion using the fast orthogonal DCT-II and DCT-III transforms [66]. Hoffman [41] forms  $\mathbf{G}^\top \mathbf{G}$  explicitly and uses a Cholesky decomposition on it. He demonstrates that for a low number of mask points the Cholesky approach applied to the Green's functions formulation can be more efficient than conjugate gradients applied to the normal equations of the classical formulation. Since we are dealing with many more mask points due to considering 4K images (in Hoffman's case this was just 4% of a  $256 \times 256$  image), it is clear that the above approach is impractical in our setting.

For 1D signals, Plonka et al. [65] have proposed a method, based on the Green's functions approach, that jointly optimizes the locations of the mask pixels as well as their tonal values. As this approach only considers 1D signals it is not applicable in our setting, and since it uses Green's functions it suffers from similar restrictions as the approach by Hoffman.

*Nested Conjugate Gradients.* A potential remedy of the memory constraint problem was proposed by Chizhov and Weickert [21] for their finite elements framework. They use a CG solver [37, 69] on the normal equations, but instead of explicitly computing the system

matrix they evaluate the matrix-vector products  $\mathbf{B}\mathbf{x}$  and  $\mathbf{B}^\top\mathbf{x}$  in an efficient manner. They rewrite  $\mathbf{B} = \tilde{\mathbf{A}}^{-1}\tilde{\mathbf{C}}$ , where  $\tilde{\mathbf{C}}$  is sparse, and where  $\tilde{\mathbf{A}}$  is sparse and symmetric positive definite. Therefore, they use a conjugate gradients solver whenever they have to compute  $\tilde{\mathbf{A}}^{-1}\mathbf{y}$  allowing them to exploit the sparsity of the problem. With this so-called nested CG approach, they achieve a memory and runtime efficient tonal optimization. In our approach, we use a similar nested strategy in our framework, where the nested iterations are replaced by an adapted version of the fast inpainting algorithm from [49].

We also note that the mesh construction and system matrix assembly for the finite element framework are not easily parallelizable, and the iterations cannot be implemented in a matrix-free fashion due to the irregular finite elements mesh. Thus, for fairness in the experiments, we consider a finite differences formulation that is easily parallelizable and allows implementing all matrix-vector products in a matrix-free fashion.

*Non-binary Mask Optimization.* Hoeltgen and Weickert have shown [40] that a thresholded non-binary mask spatial optimization [13, 20, 39, 57] can also be interpreted as a joint tonal and binary mask spatial optimization. Non-binary masks can be optimized with sophisticated non-smooth optimization strategies such as primal-dual algorithms, which then indirectly perform a tonal optimization. An extension to color images is, however, not straightforward. Additionally, while the above methods achieve very good results, they are already quite computationally intensive even for small images.

*Neural-based Approaches.* Besides model-based methods, neural networks can also be efficiently used to implement tonal optimization. Recently, Peter et al. [64] proposed the first tonal optimization neural network for homogeneous diffusion inpainting, which results in a memory efficient and fast method. While it is trained to minimize the MSE, it does not solve the least squares problem, which means that it does not necessarily obtain the best MSE. Furthermore, the network was only trained on small image resolutions and does not perform well for 4K resolution images. A naïve extension to 4K images would be impractical due to memory and computational limitations of the training process.

*Localization-based Acceleration.* Since the influence zone of a single mask pixel is mostly limited for many inpainting operators, localization strategies are an option to accelerate tonal optimization. This works especially well for perfectly localized inpainting operators such as Shepard interpolation with truncated Gaussians [2, 60], or smoothed particle hydrodynamics [23]. For less local operators, there are also methods that artificially limit the influence with a segmentation [42, 46]. Similarly, one can also restrict the support of inpainting echoes in homogeneous diffusion [41]. This essentially constructs an approximation  $\tilde{\mathbf{B}}$  of  $\mathbf{B}$  that is not fully dense anymore. Nevertheless, the number of restricted echoes which have to be computed and stored is still very large for 4K images.

In the current work we consider domain decomposition methods instead, which are a much more sophisticated way to localize computations (and thus reduces accesses to global GPU memory) without artificially imposing locality constraints on non-local operators such as homogeneous diffusion.

*Quantization.* In the context of image compression, quantization is often a factor which limits the number of available gray or color values. Including this quantization directly into the tonal optimization yields better quality than simply applying the quantization afterwards. For this discrete optimization problem several approaches have been proposed, such as pro-

jection methods [62] or stochastic strategies [55, 70]. Since we only deal with the continuous optimization problem in our paper, we do not include any of these strategies. In a full compression setting, however, one could easily integrate one of these methods.

**Singularity Suppression.** Homogeneous diffusion inpainting exhibits logarithmic singularities inherited from the continuous boundary value problem formulation in 2D [56]. Those are especially visible at lower resolutions, so while this is not really a concern for us because we consider 4K images, we nevertheless note that this issue has been tackled previously. Interpolation swapping [70] removes discs around the known data after the initial inpainting and uses a second inpainting to fill in the discs. This reduces the effect of the singularities at the mask pixels, but it modifies the inpainting operator itself. While we could also apply this in our approach, it often reduces the overall reconstruction quality due to the smoothing around the mask pixels.

**Error Balancing.** An early predecessor of tonal optimization has been proposed by Galić et al. [32] in 2008. It modifies the tonal values of each mask pixel based on the inpainting error of the neighboring pixels. This reduces the effect of singularities at mask pixels, while also improving the inpainting quality. We extend this idea both practically and theoretically, and use it as a fast way to get a good initialization for our tonal optimization algorithm.

**1.3. Paper Structure.** We give a short review of homogeneous diffusion inpainting in Section 2 and in Section 3 we give an overview of the Multigrid ORAS inpainting solver that we use in our spatial and tonal optimization methods. In Section 4, we present our Delaunay-based densification method for the spatial optimization. Section 5 provides details on our tonal optimization methods as well as our strategy for constructing a good initial guess. We evaluate our spatial and tonal optimization methods experimentally in Section 6. Finally, we conclude our paper in Section 7 and discuss our ongoing work.

**2. Homogeneous Diffusion Inpainting.** In this section we briefly review homogeneous diffusion inpainting [19], which is our inpainting method of choice and is used for all results in this paper. Homogeneous diffusion inpainting is a simple and very popular method for inpainting-based compression. It is parameter-free, allows to establish a comprehensive data selection theory, and can lead to particularly fast algorithms. It has been shown that, if the inpainting data is carefully chosen, it can achieve very good results [42, 46, 53, 54].

**2.1. Mathematical Formulation.** Let us consider a continuous grayscale image  $f : \Omega \rightarrow \mathbb{R}$ , defined on a rectangular image domain  $\Omega \subset \mathbb{R}^2$ . We store only a fraction of the full image data on a small subset  $K \subset \Omega$ . Homogeneous diffusion inpainting aims at restoring  $f$  in the inpainting domain  $\Omega \setminus K$ , by solving the Laplace equation on  $\Omega \setminus K$  with reflecting boundary conditions on  $\partial\Omega$ , and with the known data  $f|_K$  used as an interpolation constraint  $u|_K = f|_K$ :

$$(2.1) \quad -\Delta u(\mathbf{x}) = 0, \quad \mathbf{x} \in \Omega \setminus K,$$

$$(2.2) \quad u(\mathbf{x}) = f(\mathbf{x}), \quad \mathbf{x} \in K,$$

$$(2.3) \quad \partial_{\mathbf{n}} u(\mathbf{x}) = 0 \quad \mathbf{x} \in \partial\Omega,$$

where  $\partial_{\mathbf{n}} u$  denotes the derivative of  $u$  in outer normal direction  $\mathbf{n}$ .

**Discrete Setting.** For a discrete image  $\mathbf{f} \in \mathbb{R}^N$ , with  $N$  pixels, we discretize (2.1)–(2.3) with finite differences. Using an indicator function  $\mathbf{c} = \mathbf{1}_K \in \{0, 1\}^N$ , also called the *inpainting*



$mask$ , the reconstruction  $\mathbf{u}$  with homogeneous diffusion inpainting is given by the following linear system of equations:

$$(2.4) \quad \underbrace{(\mathbf{C} + (\mathbf{I} - \mathbf{C})\mathbf{L})}_{=: \mathbf{A}} \mathbf{u} = \underbrace{\mathbf{C}\mathbf{f}}_{=: \mathbf{b}},$$

where  $\mathbf{I} \in \mathbb{R}^{N \times N}$  is the identity matrix,  $\mathbf{C} := \text{diag}(\mathbf{c}) \in \mathbb{R}^{N \times N}$  is a diagonal matrix with the components of the inpainting mask on the diagonal, and  $\mathbf{L}$  is the 5-point stencil discretization of the negated Laplacian with reflecting boundary conditions. If the inpainting mask is non-empty, i.e.  $\mathbf{c} \neq \mathbf{0}$ , the inpainting problem has a unique solution since  $\mathbf{A}$  is non-singular in that case (for more details on the matrix structure see [53]). For an RGB color image the inpainting is performed on each of the three channels separately. Thus, we get three non-coupled linear systems of this type (the system matrix is the same for all of them).

*Homogeneous Diffusion Inpainting and Image Edges.* Edges are important semantic and mathematical features in images. Thus, a simple and appealing idea is to reconstruct an image from its edge information. When the Laplacian  $\mathbf{L}\mathbf{f}$  is considered as an edge detector, this idea is realized as homogeneous diffusion inpainting [19]. If  $\mathbf{L}\mathbf{f}$  is available exactly, the image can be recovered up to mean gray value as  $\mathbf{L}^+(\mathbf{L}\mathbf{f})$ , where  $\mathbf{L}^+$  is the Moore-Penrose inverse. Since  $\mathbf{L}$  has a high-pass profile,  $\mathbf{L}^+$  has a low-pass character and (2.4) fills in information smoothly between mask points.

In practice, we do not want to store  $\mathbf{L}\mathbf{f}$  exactly, leading to the sparse approximation problem with the inpainting from (2.4). Earlier approaches [1, 7, 19, 25, 34, 52, 86] for homogeneous diffusion inpainting used the pixels left and right of the edges as known data, in order to preserve them in the reconstruction. While modern approaches usually do not directly use the edges to determine the inpainting data, the optimized inpainting masks still cluster around prominent image edges. For an illustration of this effect, see Figure 12. Further theoretical justifications for choosing reconstruction data based on the Laplacian can be found in the work of Belhachmi et al. [8].

We also note that the choice of reflecting boundary conditions (2.3) is standard in image processing, as it produces the best results for the compression of natural images. In fact the matrix  $\mathbf{L}$  has eigenvectors the rows of the DCT-II transform [75], which is known to have the best energy compaction properties for natural images, out of all the DFT/DST/DCT variants.

*Alternative Inpainting Operators.* An alternative class of sparse inpainting operators use locally supported positive definite kernels [23, 60, 82]. While the latter has considerable advantages since it does not have to deal with global interactions, there are non-trivial challenges associated with this approach. The kernels come with various parameters that have to be optimized per mask point. This necessitates multiple iterations to produce a single inpainting [23], that is neither over-blurred – due to the kernel supports being too large, nor has holes – due to the kernel supports being too small.

Other options include nonlinear inpainting methods such as anisotropic diffusion inpainting [81]. Such methods can achieve state-of-the-art quality [32], however, that comes at a considerable computational cost. We have left the study of these alternatives as future work, and have focused instead on constructing the first complete framework for data optimization applicable to sparse 4K image inpainting.

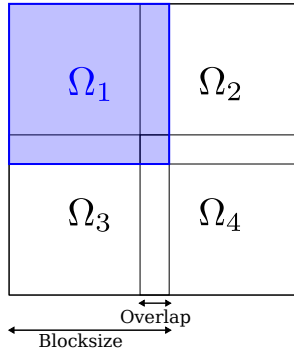


Figure 1: **Domain Decomposition Example.** The domain is divided into four overlapping subdomains. The subdomain  $\Omega_1$  is highlighted in blue.

**3. Multigrid ORAS Inpainting Solver.** To keep our manuscript self-contained, we describe the Multigrid ORAS inpainting solver that we use for the inpainting problems that occur in our proposed data optimization methods. It consists of a domain decomposition method embedded into a multigrid framework. For more details on the Multigrid ORAS inpainting solver, we refer the reader to [49].

### 3.1. Optimized Restricted Additive Schwarz Method.

The *optimized restricted additive Schwarz (ORAS)* method [74], in its discrete formulation, is an iterative technique for solving linear systems that arise from the discretization of boundary value problems, such as (2.4). It is one of the simplest domain decomposition methods [28, 78] and is well suited for parallelization. As a first step, the image domain  $\Omega$  with  $N$  pixels is divided into  $k \in \mathbb{N}$  overlapping subdomains  $\Omega_1, \dots, \Omega_k \subset \Omega$ , such that  $\cup_{i=1}^k \Omega_i = \Omega$ . An example of such an overlapping division into four subdomains is shown in Figure 1.

Starting with an initial approximation  $\mathbf{u}^0 \in \mathbb{R}^N$  that fulfills the interpolation condition  $\mathbf{C}\mathbf{u}^0 = \mathbf{C}\mathbf{f}$  at the known locations, in each iteration  $n$ , we try to correct the current approximation  $\mathbf{u}^n$  by locally computing correction terms for every subdomain. We compute the corrections by solving local variants of the global linear system

$$(3.1) \quad \mathbf{A}_i \mathbf{v}_i^n = \mathbf{R}_i \mathbf{r}^n,$$

where the right-hand side consists of the global residual  $\mathbf{r}^n = \mathbf{b} - \mathbf{A}\mathbf{u}^n$  restricted to the subdomains. We use matrices  $\mathbf{R}_i \in \mathbb{R}^{|\Omega_i| \times N}$  to restrict global vectors to the local domains by extracting the values from the subdomain  $\Omega_i$  and ignoring all values outside of it. The local system matrices  $\mathbf{A}_i$  are given by restricting the global system matrix  $\mathbf{A}$  to the subdomains  $\Omega_i$  with additional boundary conditions at the subdomain boundaries which are not part of the global image boundary. At these so-called inner subdomain boundaries, we impose mixed Robin boundary conditions, which improve the convergence speed compared to simpler Dirichlet boundary conditions [74].

The next iterate  $\mathbf{u}_{n+1}$  is given by extending the local corrections  $\mathbf{v}_i$  from the subdomain  $\Omega_i$  to the global domain  $\Omega$  and adding them to the old iterate  $\mathbf{u}_n$ :

$$(3.2) \quad \mathbf{u}^{n+1} = \mathbf{u}^n + \sum_{i=1}^k \mathbf{R}_i^\top \mathbf{D}_i \mathbf{v}_i^n$$

For the extension, we use the transposes of the restriction matrices  $\mathbf{R}_i^\top$ . However, in order to achieve convergence, we also have to weight the local corrections in the overlapping regions before adding them to the global solution [29, 33], to compensate for the fact that we add multiple corrections in the overlapping regions. To this end we define diagonal nonnegative weight matrices  $\mathbf{D}_i \in \mathbb{R}^{|\Omega_i| \times |\Omega_i|}$ , such that

$$(3.3) \quad \mathbf{I} = \sum_{i=1}^k \mathbf{R}_i^\top \mathbf{D}_i \mathbf{R}_i,$$

where  $\mathbf{I} \in \mathbb{R}^{N \times N}$  is the identity matrix of size  $N \times N$ .

**3.2. Embedding ORAS in Multigrid.** Since the ORAS method only allows communication between neighboring blocks, many iterations are necessary to spread information over large distances. This means that high frequency components of the error are reduced much faster than low frequency components, which leads to an overall slow convergence rate. As a remedy, domain decomposition methods are usually used together with a two-level scheme that computes a correction on a very coarse grid to couple all subdomains together [28, 78]. In our case, where the influence area of each mask pixel is already approximately localized, such a global coupling would be too coarse and result in a poor performance. Instead, the more fine-grained coupling of multigrid methods [14, 15, 17, 26, 36, 79, 83] can be more beneficial. Multigrid methods transfer the problem to coarser grids where the low frequencies appear as higher frequencies, which can be reduced more efficiently with iterative solvers such as Jacobi [69], Gauss-Seidel [69], or the ORAS method [74].

*Two-Grid Cycle.* We first give an overview over the simple two-grid cycle, which we then extend to use multiple resolution levels. Our two grids are the original fine grid with grid spacing  $h$ , and a coarser grid with spacing  $H = 2h$ .

We start the cycle  $k + 1$  with an approximation  $\mathbf{u}_h^k$  of the solution  $\mathbf{u}_h$  of the problem  $\mathbf{A}_h \mathbf{u}_h = \mathbf{b}_h$ , where  $\mathbf{A}_h$  is the original system matrix and  $\mathbf{b}_h$  the right-hand side on the original grid. The goal of the two-grid cycle is to find a good approximation of the true error  $\mathbf{u}_h - \mathbf{u}_h^k$ , by decimating different frequencies of the error over different grids. We reduce the high frequencies by performing a few iterations  $\vartheta_{\text{pre}}$  with a *smoother*: an iterative solver that dampens the high frequencies efficiently - e.g. damped Jacobi, Gauss-Seidel, or in our case ORAS. This results in the approximation of the solution

$$(3.4) \quad \mathbf{u}_h^{k+1/3} = \text{pre-smooth}(\mathbf{A}_h, \mathbf{b}_h, \mathbf{u}_h^k, \vartheta_{\text{pre}}).$$

With enough iterations  $\vartheta_{\text{pre}}$ , the error will have only negligible high-frequency components and we can transfer it almost perfectly to the coarser grid with a restriction matrix  $\mathbf{R}_h^H$ . While we do not know the true error in practice, we know the residual and its relation to the error:

$$(3.5) \quad \mathbf{r}_h^k = \mathbf{b}_h - \mathbf{A}_h \mathbf{u}_h^{k+1/3} = \mathbf{A}_h \mathbf{u}_h - \mathbf{A}_h \mathbf{u}_h^{k+1/3} = \mathbf{A}_h \left( \mathbf{u}_h - \mathbf{u}_h^{k+1/3} \right) = \mathbf{A}_h \mathbf{e}_h^k.$$

Instead of solving this equation on the fine grid, we transfer it to the coarser grid and solve it for the coarse error  $\mathbf{e}_H^k$  as

$$(3.6) \quad \mathbf{A}_H \mathbf{e}_H^k = \mathbf{r}_H^k.$$

Here  $\mathbf{A}_H$  is an analogue of  $\mathbf{A}_h$ , obtained by discretizing the inpainting problem on the coarser grid, and  $\mathbf{r}_H^k = \mathbf{R}_h^H \mathbf{r}_h^k$  is the coarse residual, obtained by restricting the original residual to the coarser grid. Since the matrix  $\mathbf{A}_H$  is twice smaller in each dimension compared to  $\mathbf{A}_h$ , the computational cost is also reduced. We can then transfer  $\mathbf{e}_H^k$  to the fine grid by using a prolongation matrix  $\tilde{\mathbf{e}}_h^k = \mathbf{P}_H^h \mathbf{e}_H^k$  and use it to correct our approximation of the solution:

$$(3.7) \quad \mathbf{u}_h^{k+2/3} = \mathbf{u}_h^{k+1/3} + \tilde{\mathbf{e}}_h^k = \mathbf{u}_h^{k+1/3} + \mathbf{P}_H^h \mathbf{e}_H^k.$$

A subsequent post-smoothing with  $\vartheta_{\text{post}}$  iterations is applied to smooth high frequency error components potentially introduced by the correction step:

$$(3.8) \quad \mathbf{u}_h^{k+1} = \text{post-smooth}(\mathbf{A}_h, \mathbf{b}_h, \mathbf{u}_h^{k+2/3}, \vartheta_{\text{post}}).$$

*Extension to More Resolution Levels.* We extend the two-grid cycle to multiple levels, which allows to efficiently dampen different frequencies of the error at different resolutions. The solve on the coarse level is replaced by another correction step on an even coarser level. We iterate this process recursively until the desired number of resolution levels are reached. This type of hierarchical application of the two-grid cycle is termed a *V-cycle*.

Additionally we speed up the computation even further by providing a good initialization. The latter is obtained by computing an inpainting solution on a coarser grid and prolongating it to the fine resolution. We extend this to a complete coarse-to-fine initialization strategy. While this is usually used with a complete V-cycle on each resolution level, we instead skip the V-cycles on the lower levels and just use a single pre-smoothing iteration in each lower level. The resulting reduced *full multigrid (FMG)* scheme, is depicted in [Figure 2](#). It decreases the amount of costly restriction and prolongation operations, while still offering sufficient convergence for homogeneous diffusion inpainting.

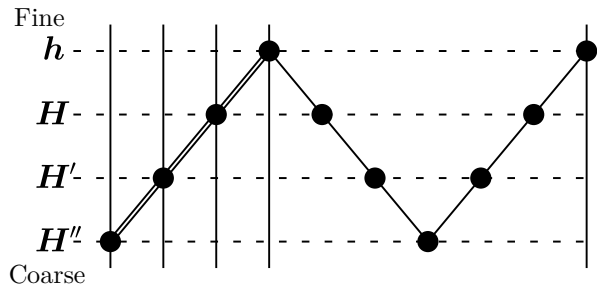


Figure 2: **Reduced Full Multigrid Scheme.** The initial guess is constructed in a coarse-to-fine manner, also known as one-way or cascadic multigrid [14]. Then we continue with additional V-cycle correction steps (a single V-cycle is visualized above).

**3.3. Implementation Details.** In our ORAS method we decompose the image domain into multiple overlapping blocks of size  $32 \times 32$  pixels with an overlap of 6 pixels. These values are optimized for our *Nvidia GeForce GTX 1080 Ti* GPU, which results in 36852 local problems in each iteration of the ORAS method for a 4K color image on the finest resolution layer. The local problems are solved using a simple conjugate gradient algorithm [69]. We stop the local CG iterations on a block when the squared 2-norm of the residual has been reduced to a fixed fraction of the squared global residual norm. Compared to a stopping criterion based on the local relative residual norm, this leads to a more uniform convergence, since all blocks have the same squared residual norm after each ORAS iteration. This also avoids using unnecessarily many CG iterations in blocks that are already sufficiently converged.

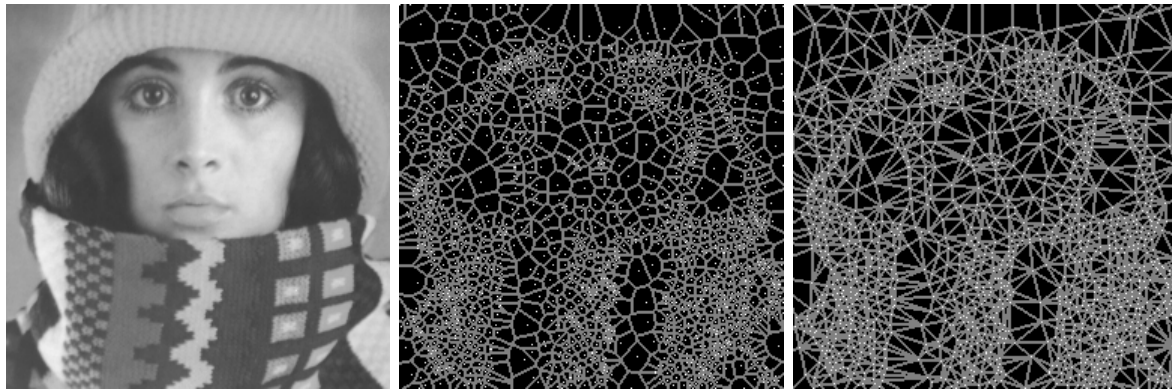
For our multigrid embedding, we use a single V-cycle on the finest level with a single ORAS iteration as pre- and post-smoothing. The number of resolution levels is chosen, such that the coarsest level consists of a single ORAS block. For the restriction of the inpainting mask we consider a coarse pixel to be a known pixel, if at least one of its four corresponding fine resolution pixels is a known pixel. For each coarse mask pixel its value is obtained as an average over the corresponding fine resolution pixel values. This method offers the advantage of increasing the mask density with each level, which in turn leads to faster convergence at the coarser levels.

**4. Spatial Optimization.** The problem of spatial optimization or mask optimization for homogeneous diffusion inpainting consists of finding a binary mask  $\mathbf{c} \in \{0, 1\}^N$ , that results in a reconstruction minimizing some error metric such as the  $L_2$  error  $\|\mathbf{u}(\mathbf{c}, \mathbf{f}) - \mathbf{f}\|_2$ , under the constraint  $\|\mathbf{c}\|_1 = \lfloor d \cdot N \rfloor$  on the number of mask pixels. Here  $\|\cdot\|_1$  denotes the 1-norm of  $\mathbf{c}$  (i.e. the number of mask pixels), and  $d$  is a user-specified target density, which in a compression setting will be a function of the compression ratio.

**4.1. Densification.** Our spatial optimization method is based on the Voronoi-based densification strategies by Daropoulos et al. [23] and Jost et al. [45], and the Delaunay-based strategy by Chizhov and Weickert [21], which combine densification with ideas from error map dithering [50].

Densification methods for spatial optimization iteratively add mask pixels in areas with high inpainting errors, starting with some initial mask. In each iteration, an inpainting  $\mathbf{u}$  is computed from the current mask, and an error map is constructed as  $\mathbf{e} = |\mathbf{u} - \mathbf{f}|^2$  [50]. As our goal is to minimize the  $L_2$  error, we use the squared error. Then one tries to balance the error at each iteration by introducing new pixels wherever the error is highest in the current error map. An issue with a naïve implementation of such an approach is that if we introduce more than one pixel per iteration, the new pixels may clump around a high error area. The problem lies in the fact that if new pixels are introduced at the locations of highest pointwise error, then every new pixel fails to account for the effect of all other new pixels.

In practice, it is paramount that we introduce multiple pixels per iteration in order to keep the number of inpaintings and thus computational cost low. A remedy to this is to introduce a mask-adaptive partition, that approximates the influence region of potential new pixels, and to insert only a single pixel per cell. We can then think of the densification as an error balancing process, that tries to construct a partition such that the error is close to equal in each cell.



(a) original image *trui*      (b) Voronoi tessellation      (c) Delaunay triangulation

Figure 3: **Voronoi and Delaunay Example on *trui* with a 2% Mask Density.**

*Mask-Adaptive Partition.* The Voronoi tessellation [6] offers a reasonable approximation of the influence zones of the already added mask pixels, as discussed in [23], but in densification we are interested in the influence regions of potential new pixels. This means that ideally the partition of the space would have the current mask pixels as vertices, and the cells would be bounded by those. The dual of a Voronoi diagram - the Delaunay triangulation [6] - can be used to partition the domain in such a way. Given the mask pixels as vertices, it produces the triangulation that maximizes the minimum of all angles in the triangulation. This has the desirable effect that triangles are not elongated, and thus provide better approximations to the influence areas of isotropic operators such as homogeneous diffusion. Figure 3 shows an example of a Voronoi diagram and its corresponding Delaunay triangulation for an optimized inpainting mask with a density of 2%.

*Algorithm.* To start the densification, we need a non-empty initial mask  $\mathbf{c}$  with a small amount of mask pixels in order to compute the first inpainting. We may obtain such an initial guess by using uniform random sampling or with another spatial optimization method, for example the Belhachmi approach [8]. In each iteration, we compute an inpainting  $\mathbf{u} = \mathbf{A}^{-1}\mathbf{C}\mathbf{f}$  from the mask in the current iteration. We can then compute the error map  $\mathbf{e} = |\mathbf{u} - \mathbf{f}|^2$ , partition the domain using a Delaunay triangulation with the current mask pixels as vertices, and then integrate the error map within each triangle  $\mathcal{T}_i$  to obtain the accumulated errors  $e_{\mathcal{T}_i}$ :

$$(4.1) \quad e_{\mathcal{T}_i} = \sum_{j \in \mathcal{T}_i} e_j = \sum_{j \in \mathcal{T}_i} |u_j - f_j|^2.$$

Since we need to introduce multiple pixels in a single iteration, we distribute them so that we insert at most one per triangle, and we choose the triangles in order of decreasing triangle error  $e_{\mathcal{T}_i}$ . The pixels are placed at the location of highest pointwise error within the triangles. This allows us to avoid clumping while at the same time having a scale-adaptive partition. We iterate this process until we reach the desired mask density. Algorithm 4.1 describes the Delaunay densification process, and Figure 4 illustrates it.

*Comparison to Spatial Optimization for Delaunay Based Inpainting.* Various methods rely on (at a first glance) similar strategies for greedily optimizing the inpainting mask. Specifically

in the context of the used Delaunay partition, the work of Demaret et al. [24], Adams [3], and Marwood et al. [55] use linear splines over Delaunay triangulations for sparse image reconstruction. Their methods are specifically adapted to the linear splines Delaunay inpainting that is motivated from the desire of not storing the connectivity of a triangulation, while our method could easily be generalized for other inpainting methods. Our method is also more sophisticated, as we integrate the errors over the adaptive partition as a predictor for the potential incurred error from removing or adding a mask pixel. Last but not least, our method is also significantly faster, as their method requires approximately 4 minutes for 23,092 initial data points, which is about 3 times lower than for a  $256 \times 256$  image.

---

**Algorithm 4.1** Delaunay Densification
 

---

**Input :** Original image  $\mathbf{f}$ , number of iterations  $n$ , number of mask pixels added in first iteration  $m_0$ , factor to increase the number of mask-pixels added per iteration  $t$

**Output :** Inpainting mask  $\mathbf{c}$ , reconstruction  $\mathbf{u}$

**Initialize:** Initial mask  $\mathbf{c}$  with a small number of mask pixels

- 1: **for**  $i = 1$  **to**  $n - 1$  **do**
  - 2:   Construct the Delaunay triangulation  $\{\mathcal{T}_j\}$  of the current mask pixels.
  - 3:   Compute the inpainting  $\mathbf{u} = \mathbf{A}^{-1}\mathbf{C}\mathbf{f}$  and the error map  $\mathbf{e} = |\mathbf{u} - \mathbf{f}|^2$ .
  - 4:   Compute the triangle errors  $\forall j, e_{\mathcal{T}_j} = \sum_{k \in \mathcal{T}_j} e_k$ .
  - 5:   Compute the number of pixels to be added  $m_i = t \cdot m_{i-1}$ .
  - 6:   Find the  $m_i$  Delaunay triangles  $\{\mathcal{T}_{j_k}\}_{k=1}^{m_i}$  with the highest errors  $\{e_{\mathcal{T}_{j_k}}\}_{k=1}^{m_i}$ .
  - 7:   For each triangle in  $\{\mathcal{T}_{j_k}\}_{k=1}^{m_i}$  find the pixel with highest error and add it to  $\mathbf{c}$ .
  - 8: **end for**
- 

**4.2. Implementation Details.** Here we discuss implementation details that improve the mask construction process from both a quality and runtime perspective.

*Image-adaptive Initial Mask.* For the initial mask in the first iteration, both [23] and [21] distribute the mask pixels uniformly at random. If we use only a very small amount of mask pixels in the initial mask, it does not have a substantial impact on the final densification result. However, as the initial mask density increases (i.e. as the number of densification steps decrease) the impact on the final result also increases. Generally, a uniform random mask is not optimal, as it is not adapted to image structures in any way. A much better distribution can be achieved by choosing the local mask density to be proportional to the Laplacian magnitude, as proposed by Belhachmi et al. [8]. They use a Floyd-Steinberg dithering [31] on the Laplacian magnitude of the reference image, however, such error diffusion algorithms are not well suited for GPU parallelization. Instead, we use a simple random dithering on the Laplacian magnitude - we do a biased coin flip for every pixel to decide whether it should become a mask pixel - with pixel probabilities proportional to the Laplacian magnitude. While by itself this results in a worse reconstruction quality compared to Floyd-Steinberg dithering, the quality degradation in a Delaunay densification process is negligible, and the greater efficiency more than pays off for it.

*Number of New Pixels per Iteration.* In [23], the authors add only a small number of mask pixels per densification iteration, which results in a large number of iterations and thus a long

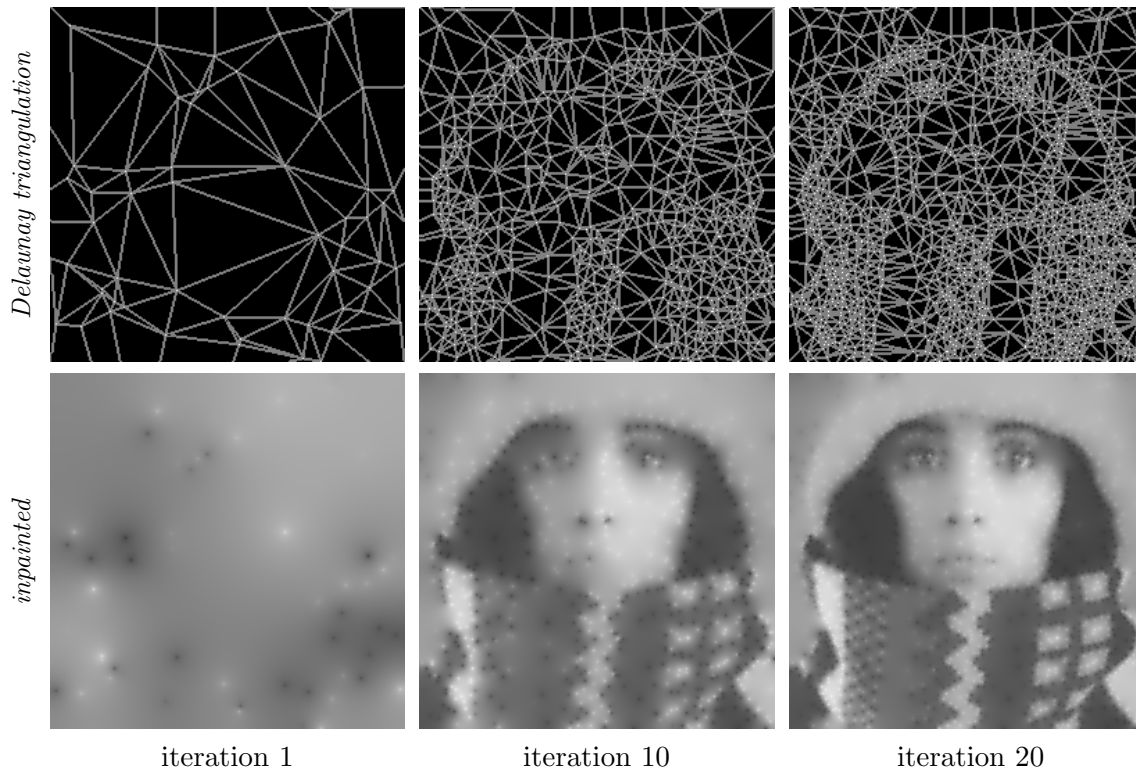


Figure 4: **Delaunay Densification Example on *trui* with a 2% Mask Density.**

runtime. Chizhov and Weickert [21] regard the number of iterations as a quality-efficiency trade-off parameter, and they fix it between 30 and 100 iterations depending on the intended goals. They introduce the exact same number of mask pixels in each iteration. We relax this restriction by allowing the number of added mask pixels per iteration to change during the densification. We specify the number of iterations  $n$  and a multiplicative factor  $t$ , with which we decrease or increase the number of added mask pixels in each iteration. For a fixed factor  $t$  and a fixed number of iterations  $n$ , we compute the number of pixels added in the first iteration, such that the desired density is achieved after exactly  $n$  iterations.

By using our multigrid ORAS solver to compute the inpainting in each iteration, we are able to perform up to 20 iterations in under 0.5 seconds with our Delaunay densification.

***Delaunay Triangulation Construction.*** Besides the computation for the inpainting reconstructions, the runtime is also determined by the construction of the Delaunay partition. For an efficient implementation we generate the Delaunay triangulation from its corresponding Voronoi diagram. We can efficiently compute the latter on the GPU with the Jump Flood Algorithm [68] (JFA). While this does not necessarily give a pixel-perfect Voronoi tessellation, it generates a very good approximation.

JFA uses several iterations to construct the Voronoi diagram. More specifically the number depends on the maximal distance between the mask points. As our densification progresses, the mask becomes denser and this distance decreases. This allows us to use fewer iterations





(a) original image *trui*      (b) no tonal opt.: 141.48 MSE      (c) tonal opt.: 63.78 MSE

Figure 5: **Tonal Optimization Example on *trui* with an Optimized Mask of 2% Density.** The tonal optimization enhances the contrast and significantly improves the MSE.

in JFA, which speeds up the process.

**5. Tonal Optimization with Domain Decomposition.** Homogeneous diffusion inpainting interpolates the values at the mask pixels from the reference image. By replacing the interpolation constraint with a best approximation condition over the whole image, we can obtain the optimal MSE given a specific image and mask. Solving this approximation problem is termed *tonal optimization*. Figure 5 demonstrates the importance of tonal optimization for homogeneous diffusion inpainting. It significantly improves the sharpness of edges and leads to better grayscale or color values in homogeneous regions, which results in a huge improvement of the MSE.

Since the homogeneous diffusion inpainting operator  $\mathbf{B} := \mathbf{A}^{-1}\mathbf{C}$  is a linear operator with respect to the grayscale or color values  $\mathbf{f}$ , we can formulate the tonal optimization as a linear least squares optimization problem, given a fixed inpainting mask  $\mathbf{c}$ . We can replace the stored values at the mask  $\mathbf{C}\mathbf{f}$  by  $\mathbf{C}\mathbf{g}$ , where we optimize  $\mathbf{g}$  to give the best approximation w.r.t. the MSE:

$$(5.1) \quad \underset{\mathbf{g} \in \mathbb{R}^N}{\operatorname{argmin}} \|\mathbf{f} - \mathbf{B}\mathbf{g}\|_2^2.$$

Since grayscale or color values  $\mathbf{g}_i$  at pixels  $i \in \Omega \setminus K$  outside the inpainting mask  $\mathbf{c}$  have no influence on the inpainting result we simply set them to 0. The choice of the 2-norm is especially appealing here (and rather standard in image processing) as it results in a linear least squares problem. Other options that result in linear least squares would include weighted 2-norms  $\|\cdot\|_{\mathbf{G}}$ , however, in our case we want the reconstructed image  $\mathbf{B}\mathbf{g}$  to look as close as possible to the original  $\mathbf{f}$  overall, so introducing a weighting matrix does not provide any benefits. A weighted norm could be used potentially in a foveated rendering setting.

In the following subsection we discuss how we solve the resulting least squares problem efficiently.

**5.1. CGNR Solver for Tonal Optimization.** The global minima of the minimization problem (5.1) satisfy the normal equations, which in our case are given by the following positive

semi-definite linear system of equations:

$$(5.2) \quad \mathbf{B}^\top \mathbf{B} \mathbf{g} = \mathbf{B}^\top \mathbf{f}.$$

Since it is always symmetric and positive semi-definite, a standard conjugate gradient method (CG) [37, 69] can be used to solve it. Each iteration of the CG algorithm requires a matrix-vector multiplication and the evaluation of a few inner products.

*Matrix-Vector Products.* While it is possible to compute this matrix explicitly, storing it requires memory that scales quadratically with the number of pixels. This becomes unfeasible for large images. To achieve high memory and computational efficiency, we keep our methods matrix-free and utilize the sparsity of the inpainting matrix  $\mathbf{A}$ . Therefore, we implement the matrix-vector products by solving linear systems involving  $\mathbf{A}$  instead of precomputing  $\mathbf{B}$ .

To compute the matrix-vector product  $\mathbf{z} = \mathbf{B}^\top \mathbf{B} \mathbf{x}$  we first have to solve  $\mathbf{A} \mathbf{y} = \mathbf{C} \mathbf{x}$  (for the step  $\mathbf{y} = \mathbf{B} \mathbf{x} = \mathbf{A}^{-1} \mathbf{C} \mathbf{x}$ ), and then we have to solve  $\mathbf{A}^\top \mathbf{C} \mathbf{z} = \mathbf{y}$  (for the step  $\mathbf{z} = \mathbf{B}^\top \mathbf{y} = \mathbf{C} \mathbf{A}^{-\top} \mathbf{y}$ ). This leads to a nested problem structure with the outer tonal optimization problem and the two inner inpainting problems in each iteration.

The linear system corresponding to the product  $\mathbf{B}^\top \mathbf{w}$  involves the non-symmetric matrix  $\mathbf{A}^\top$ , which does not reduce to a symmetric system in the same way as  $\mathbf{A} \mathbf{x} = \mathbf{b}$ . Thus, we cannot solve it with the CG algorithm or the multigrid ORAS inpainting solver. As a remedy we use a symmetrized inpainting matrix  $\tilde{\mathbf{A}}$  together with a modified  $\tilde{\mathbf{C}}$ , such that  $\tilde{\mathbf{A}} \mathbf{u} = \tilde{\mathbf{C}} \mathbf{f}$  has the same solution as  $\mathbf{A} \mathbf{u} = \mathbf{C} \mathbf{f}$ . We can derive them with the following transformations, by using the fact that  $\mathbf{C} \mathbf{u} = \mathbf{C} \mathbf{f}$ , as the inpainting solution and the original image coincide at the mask pixels:

$$\begin{aligned} (\mathbf{C} + (\mathbf{I} - \mathbf{C})\mathbf{L}) \mathbf{u} &= \mathbf{C} \mathbf{f} \\ \mathbf{C} \mathbf{u} + (\mathbf{I} - \mathbf{C})\mathbf{L}(\mathbf{I} - \mathbf{C} + \mathbf{C})\mathbf{u} &= \mathbf{C} \mathbf{f} \\ \mathbf{C} \mathbf{u} + (\mathbf{I} - \mathbf{C})\mathbf{L}(\mathbf{I} - \mathbf{C})\mathbf{u} + (\mathbf{I} - \mathbf{C})\mathbf{L}\mathbf{C}\mathbf{u} &= \mathbf{C} \mathbf{f} \\ \mathbf{C} \mathbf{u} + (\mathbf{I} - \mathbf{C})\mathbf{L}(\mathbf{I} - \mathbf{C})\mathbf{u} + (\mathbf{I} - \mathbf{C})\mathbf{L}\mathbf{C}\mathbf{f} &= \mathbf{C} \mathbf{f} \\ \underbrace{(\mathbf{C} + (\mathbf{I} - \mathbf{C})\mathbf{L}(\mathbf{I} - \mathbf{C}))}_{=:\tilde{\mathbf{A}}} \mathbf{u} &= \underbrace{(\mathbf{C} - (\mathbf{I} - \mathbf{C})\mathbf{L}\mathbf{C})}_{=:\tilde{\mathbf{C}}} \mathbf{f}. \end{aligned}$$

Consequently, we are able to replace the linear systems with their symmetrized variants, meaning we only have to solve symmetric linear systems. Solving both the outer problem and the inner symmetrized inpainting problems with a CG solver leads to the nested CG approach from Chizhov and Weickert [21].

We note that one could also apply other solvers for symmetric problems to solve  $\tilde{\mathbf{A}} \mathbf{u} = \tilde{\mathbf{C}} \mathbf{f}$ , such as the conjugate residual (CR) method, the minimal residual (MINRES) solver [58], or the symmetric LQ (SYMMLQ) algorithm [58]. However, while those methods minimize the residual faster compared to conjugate gradients, and work for indefinite systems, CG remains the fastest w.r.t. minimizing the error to the solution  $\mathbf{u}^*$  for our problem. In our case  $\tilde{\mathbf{A}}$  is positive definite as long as  $\mathbf{c} \neq \mathbf{0}$ , so we leverage this fact by using CG.

*Improvements.* We improve the nested CG approach in two ways. First, we replace the inner CG solvers for the two inpainting problems by the multigrid ORAS inpainting solver, which improves the runtime by more than a factor of 4. Secondly, we propose to replace the

outer CG solver with CGNR, a variant of CG for the normal equations [12, 37, 69]. Besides better numerical stability compared to CG, CGNR also has the advantage that the original inpainting residual  $\mathbf{r} = \mathbf{f} - \mathbf{A}\mathbf{u}$ , and hence the MSE, is available in each iteration. Because we want to optimize the MSE, a stopping criterion based on the relative improvement of the MSE in an iteration is better suited for our purposes than the standard stopping criterion based on the 2-norm of the residual of the normal equations  $\|\mathbf{B}^\top(\mathbf{f} - \mathbf{B}\mathbf{g})\|_2$ .

**5.2. RAS Solver for Tonal Optimization.** Since the influence zone of each mask pixel is effectively local, as is seen in [41], this also holds for the system matrix of the normal equations. The system matrix has non-negligible entries only for pairs of mask pixels that are near each other. All entries outside a local neighborhood are nearly zero and can be ignored without introducing large errors. This leads to a sparse matrix structure with localized connections, which is very suitable for domain decomposition methods.

*Domain Decomposition.* Taking into account the above, we solve the normal equations with a domain decomposition method instead of CGNR. We adapt a *restricted additive Schwarz (RAS)* method [18], which is similar to the one used in the multigrid ORAS inpainting solver. Similar to the inpainting solver, we subdivide the image domain  $\Omega$  into  $k \in \mathbb{N}$  overlapping subdomains  $\Omega_1, \dots, \Omega_k \subset \Omega$ , such that  $\cup_{i=1}^k \Omega_i = \Omega$ . The resulting RAS tonal optimization is given in Algorithm 5.1. It consists of three steps that are iterated until the method is sufficiently converged.

---

**Algorithm 5.1** RAS for Tonal Optimization

---

1. Compute the global residual  $\mathbf{r}^n \in \mathbb{R}^N$ :

$$(5.3) \quad \mathbf{r}^n = \mathbf{B}^\top(\mathbf{f} - \mathbf{B}\mathbf{g}^n)$$

2. For  $i \in \{1, \dots, k\}$  solve for a local correction  $\mathbf{v}_i^n$ :

$$(5.4) \quad \mathbf{B}_i^\top \mathbf{B}_i \mathbf{v}_i^n = \mathbf{R}_i \mathbf{r}^n$$

3. Update  $\mathbf{g}^n$  with the weighted and extended local corrections  $\mathbf{v}_i^n$ :

$$(5.5) \quad \mathbf{g}^{n+1} = \mathbf{g}^n + \sum_{i=1}^k \mathbf{R}_i^\top \mathbf{D}_i \mathbf{v}_i^n$$


---

First we compute the global residual  $\mathbf{r}^n$ . This involves the application of the system matrix. As in Subsection 5.1 we evaluate the matrix-vector products without explicitly forming the matrix, by solving two inner inpainting problems. As the inpainting solution changes only slightly from one iteration to the next, it can be used as a good initialization for the next inpainting. This allows us to skip the initialization phase in the full multigrid ORAS inpainting solver and start directly with a V-cycle at the finest resolution level, which improves the runtime of both inpaintings significantly. This is an advantage of RAS compared to CGNR, where we apply the system matrix only to conjugate vectors, which change more from one iteration to the next, and thus cannot be used as a good initialization.

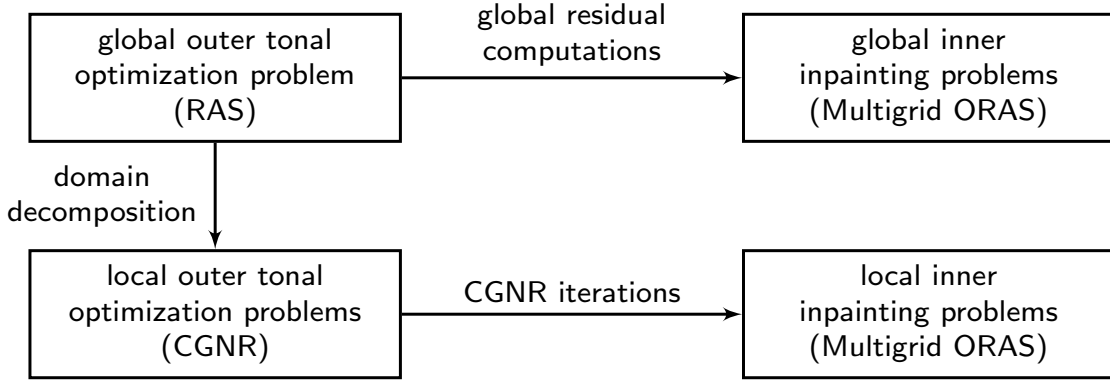


Figure 6: **RAS Tonal Optimization Schematic.** The RAS tonal optimization method consists of four problems types, which are solved with different solvers.

**Local Normal Equations.** In the second step, we compute local corrections  $\mathbf{v}_i^n$  to the residual for each subdomain, obtained by solving local versions of the global normal equations. The right-hand side for each subdomain  $\Omega_i$  is given by restricting the residual  $\mathbf{r}^n$  with the same restriction operator  $\mathbf{R}_i$  as in the inpainting case. For the local system matrix, we individually restrict the symmetrized inpainting matrix  $\tilde{\mathbf{A}}$  to  $\tilde{\mathbf{A}}_i$  and the modified mask  $\tilde{\mathbf{C}}$  to  $\tilde{\mathbf{C}}_i$ . By restricting  $\mathbf{C}$ ,  $\mathbf{L}$ , and  $\mathbf{I}$  individually, we get homogeneous Neumann boundary conditions at all subdomain boundaries for the inner inpainting problems.

In the third step, we weight the local corrections  $\mathbf{v}_i^n$  with weights  $\mathbf{D}_i$  and add them to the global solution  $\mathbf{g}^n$ . The weights  $\mathbf{D}_i$  have to fulfill the partition of unity property in order to guarantee convergence.

**Solver Structure.** Overall our RAS method consists of four types of problems, which are shown in Figure 6. Our *global tonal optimization* problem is solved with RAS which includes two *global inner inpainting* problems per iteration to compute the global residual. As with our spatial optimization method, we solve them with the multigrid ORAS inpainting solver. For each domain decomposition block in the RAS solver we also get *local tonal optimization* problems which we solve with CGNR. These again include two *local inner inpainting* problems per iteration that we solve with the same multigrid ORAS inpainting method.

For the domain decomposition we use blocks of size  $64 \times 64$ , an overlap of 6 pixels and a simple averaging for mask pixels in the overlap. The size of the blocks should be a multiple of 32 due to the architecture of our GPU in order to achieve a good performance. We found that a block size of 64 and an overlap of 6 pixels between them is optimal for our GPU, as the blocks are still quite small while the average number of mask pixels per block and the overlap is sufficiently large for a good convergence towards the global solution.

**5.3. Voronoi Initialization.** Typically one would initialize CGNR or RAS for tonal optimization at the mask pixels with the values from the original image. While this is a reasonable first guess, an even better initialization can significantly improve the runtime of the tonal optimization. Therefore, we propose an initialization strategy inspired by an early predecessor of tonal optimization by Galić et al. [32]. Along with the algorithmic improvements, we also

provide a new theoretical perspective that subsumes both our method and the one of Galić et al..

*Error Balancing.* The approach by Galić et al. [32] does not solve the full tonal optimization problem, but it already leads to a significant quality improvement, compared to the non-optimized inpainting result. The idea is to adjust the tonal value of each mask pixel, by adding the average signed inpainting error of its neighbors to it:

$$(5.6) \quad \mathbf{g}_i = \mathbf{u}_i + \frac{1}{|\mathcal{N}(i)|} \sum_{j \in \mathcal{N}(i)} (\mathbf{f}_j - \mathbf{u}_j) \quad \text{for all } i \in K,$$

where  $\mathcal{N}(i)$  denote all direct neighbors of mask pixel  $i$ , including the diagonal ones and itself. Since homogeneous diffusion inpainting suffers from logarithmic singularities at the mask pixels, their color values differ significantly from the color values of the surrounding pixels. This leads to a large error in the neighborhood, which this method tries to compensate for by modifying the value at the mask pixel.

*Interpolation of Local Averages.* We interpret the above method as performing a single step towards making mask pixels interpolate the averages over the neighborhoods. This is not unlike the local average constraints used in [45]. Taking this interpretation as a starting point we can rewrite the averaging around the mask pixels with a weight matrix  $\mathbf{W} \in \mathbb{R}^{N \times N}$  to generalize the method. Instead of interpolating  $\mathbf{f}$  at the mask pixels, we want to interpolate the averages  $(\mathbf{W}\mathbf{f})_i$  around the mask pixels, which leads to the following constraints:

$$(5.7) \quad \mathbf{C}\mathbf{W}\mathbf{A}^{-1}\mathbf{C}\mathbf{g} =: \mathbf{C}\mathbf{W}\mathbf{u} = \mathbf{C}\mathbf{W}\mathbf{f}.$$

We solve (5.7) with a modified Richardson iteration:

$$(5.8) \quad \mathbf{C}\mathbf{g}^{k+1} = \mathbf{C}\mathbf{g}^k + \tau(\mathbf{C}\mathbf{f} - \mathbf{C}\mathbf{W}\mathbf{A}^{-1}\mathbf{C}\mathbf{g}^k).$$

In our framework the original method by Galić et al. corresponds to a single Richardson step with step size  $\tau = 1$ , and a very simple  $\mathbf{W}$ . By performing multiple steps instead, we can further improve the MSE. We pick  $\tau$  so that the scheme is stable in the 2-norm:  $\|\mathbf{C} - \tau\mathbf{C}\mathbf{W}\mathbf{A}^{-1}\mathbf{C}\|_2 < 1$ . We propose to stop the iteration once the MSE starts to increase. This can happen, as the average interpolation problem is not the same as the tonal optimization problem, but is only an approximate surrogate for it.

*Voronoi Diagram Average.* To get a closer surrogate to the tonal optimization problem, we propose to use a better approximation of the influence zone of each mask pixel. As discussed in Section 4, the cells in the Voronoi diagram offer a reasonable approximation of the influence zones of the inpainting echoes. Thus, we propose to replace the direct neighbors in  $\mathbf{W}$  with the neighbors in the Voronoi cell of each mask pixel. Furthermore, we also introduce a weighting, so that we down-weight pixels that are further away from the corresponding mask pixel and thus less important for the optimization. This leads to an improved approximation of the influence zones.

**6. Experiments.** After mentioning the technical details of our experimental setup in Section 6.1, we show the results of our spatial optimization method in Subsection 6.2 and the results for our domain decomposition tonal optimization framework in Subsection 6.3.



Figure 7: Our twelve test images of 4K resolution. Photos by J. Weickert.

**6.1. Experimental Setup.** For the experimental evaluation of our Delaunay densification spatial optimization method, we compare against the analytic approach (AA) by Belhachmi et al. [8], probabilistic sparsification (PS) [54], with (PS+NLPE) and without nonlocal pixel exchange, and the most recent neural approach by Schrader et al. [71]. The analytic approach is implemented with Floyd-Steinberg dithering [31] of the Laplacian magnitude. To ensure fair comparisons, PS and NLPE are both implemented on the GPU with the same multigrid ORAS inpainting solver that we use for our methods. For PS we use candidate fractions  $p = 0.3$  and  $q = 0.005$ , and NLPE is run for five cycles. As the neural approach requires more than 20 GB of graphics memory for runtime tests, we exclude them in our runtime comparison.

To evaluate our tonal optimization methods, we compare against a parallel GPU implementation of CGNR with CG inpainting, based on the nested CG approach by Chizhov and Weickert [21]. We adapt this approach by replacing CG with CGNR, and the finite elements with finite differences, as this is better suited for an efficient parallel GPU implementation. We exclude other tonal optimization approaches, such as the Green’s function approach [41]

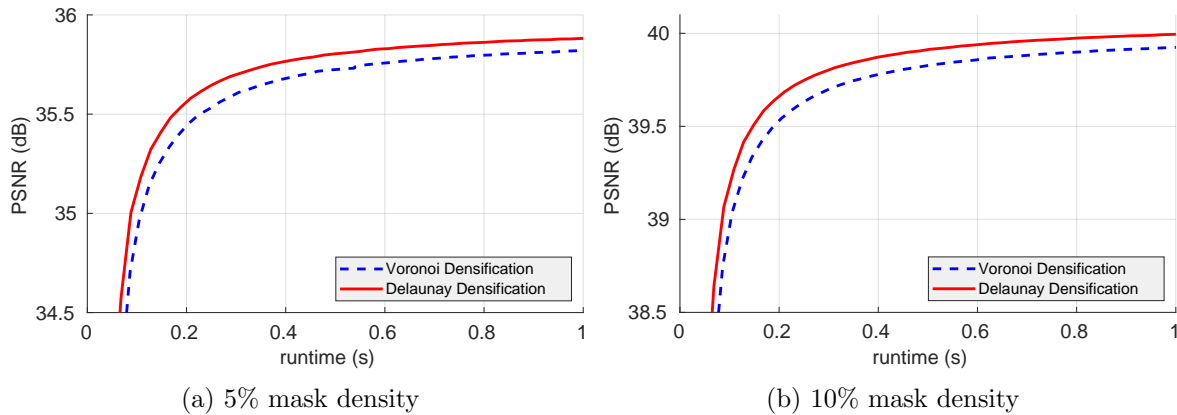


Figure 8: **Comparison between Voronoi Densification and Delaunay Densification.** Results for a mask density of 5% (a) and 10% (b). The Delaunay-based approach clearly outperforms the Voronoi-based one at all times by about 0.1 dB.

or the inpainting echo approach [54], because they either use too much memory for 4K images or they are not well-suited for parallelization. All our experiments were conducted on an *AMD Ryzen 5900X@3.7GHz* and an *Nvidia GeForce GTX 1080 Ti* GPU. Tests are performed on twelve representative 4K images containing scenes of nature with a varying amount of texture, and coarse and fine structures (see Figure 7).

**6.2. Spatial Optimization Experiments.** In Figure 8 we compare a Voronoi-based densification with a Delaunay-based one for mask densities of 5 and 10%, by varying the number of densification iterations. Since Voronoi and Delaunay densification have a different runtime per iteration, we compare the PSNR against the total runtime instead of the number of iterations. We observe that for both densities, the Delaunay densification outperforms Voronoi densification by approximately 0.1 dB. This suggests that the Delaunay triangulation is in general better suited for a densification approach than the Voronoi tessellation.

*Initial Mask and Iteration Count.* In Figure 9(a) we evaluate the impact of the choice of the initial mask on our Delaunay densification. We compare a uniform random initial mask with a Laplacian magnitude sampled initial mask. We use the same number of initial mask pixels and add a constant amount of new pixels in each iteration for both masks. We observe that for a small amount of iterations the Laplacian magnitude approach results in a significantly higher PSNR, while the difference becomes smaller the more iterations are used. This can be explained with the fact that fewer mask pixels are introduced per iteration if we have a larger numbers of iterations, which reduces the impact of the initial mask. It also shows that the improvement per iteration becomes quite small for iterations beyond 20, while the additional runtime for each iteration is approximately constant as each requires exactly one inpainting. Thus 20 iterations seem to be a good trade-off between runtime and reconstruction quality.

*Number of Mask Pixels per Iteration.* Figure 9(b) shows the effect of increasing or decreasing the number of mask pixels that are added per iteration during the densification with a constant factor  $t$ . For a uniform random initial mask we observe that adding a constant amount of pixels in each iteration is not the optimal strategy. By increasing the number of added pixels

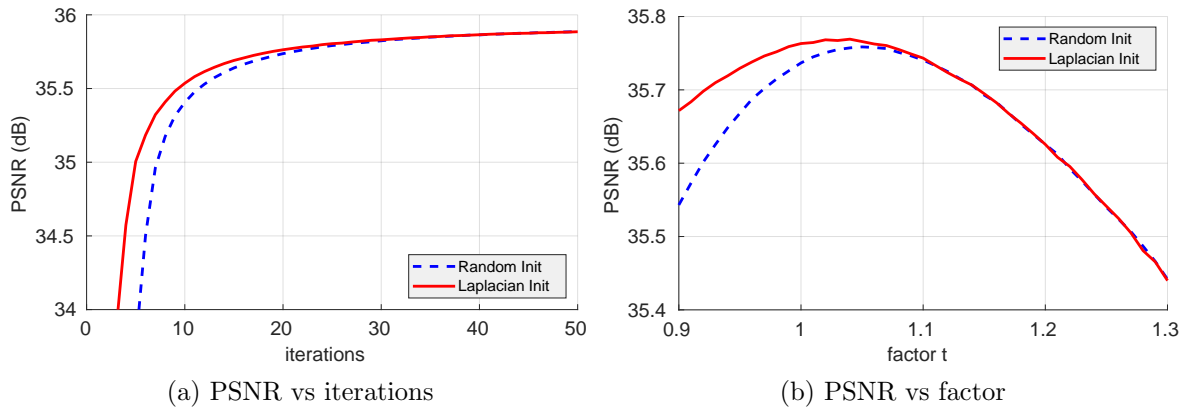


Figure 9: **Comparison of Delaunay Densification with Different Initial Iterations.** Results for a mask density of 5%. **(a)** A dithered Laplacian magnitude as an initial mask improves the PSNR significantly compared to a uniform random initialization, especially for a low number of iterations. **(b)** The random initialization benefits clearly from increasing the number of mask pixels added per iteration, while for the Laplacian initialization a constant number of mask pixels is very close to the optimum.

by a factor of  $t = 1.08$  or 8% in each iteration, we can improve the PSNR by 0.05 dB. With a sampled Laplacian magnitude as an initial mask, however, the optimal factor is only  $t = 1.03$  and the improvement compared to a constant number of pixels is less than 0.01 dB. These results also reinforce the conclusion that the Laplacian magnitude yields a suitable initial mask and suggests only slightly increasing the number of pixels added per iteration. Since the difference between adding a constant number of pixels and the optimal strategy is negligible, for simplicity we use a constant number of pixels for the rest of our experiments.

*Performance Evaluation.* We evaluate the runtimes in Figure 10(b). While the inferior analytic approach is clearly the fastest, our method is the second fastest with an average runtime of around 0.4 seconds. We achieve this by restricting our densification to 20 iterations, which still produces masks of very high quality. Compared to PS and PS+NLPE we are several orders of magnitude faster, since they both require thousands of inpaintings. For the neural approach we cannot generate any runtime results on our GPU due to memory restrictions, but the runtimes reported by Schrader et al. [71] are quite similar to the results of our approach, albeit a bit faster for densities below 3%. As they are obtained with a significantly more powerful GPU, our method should be faster on a similar GPU. Furthermore, our method has the advantage of needing significantly less GPU memory.

*Qualitative Evaluation.* The qualitative evaluation of the spatial optimization methods in Figure 10(a) shows that with just 20 densification iterations our Delaunay densification approach (DD) already consistently outperforms all its competitors on all tested mask densities. It even surpasses the recent neural approach by Schrader et al. [71] by at least 0.75 dB. Compared to the model-based competitors our method is especially well-suited for lower mask densities, which are the most interesting for inpainting-based compression.

**Here our method outperforms the analytic approach by more than 6 dB, PS by more than 3.8, and PS+NLPE by more than 2.6 dB.** This suggests that densification



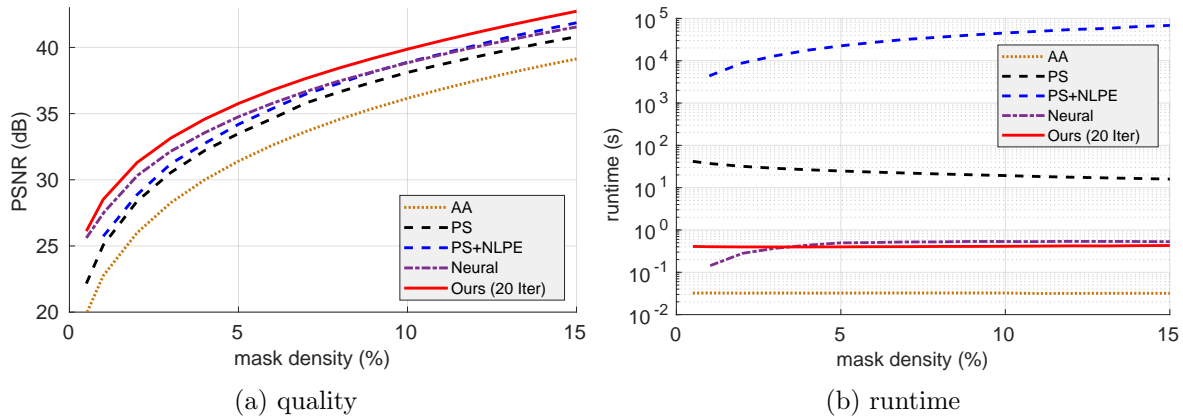


Figure 10: **Spatial Optimization Comparison.** Whilst the analytical approach [8] is the fastest, its generated masks are clearly inferior. Our Delaunay densification method is only slightly slower, but consistently outperforms all its competitors in terms of quality.

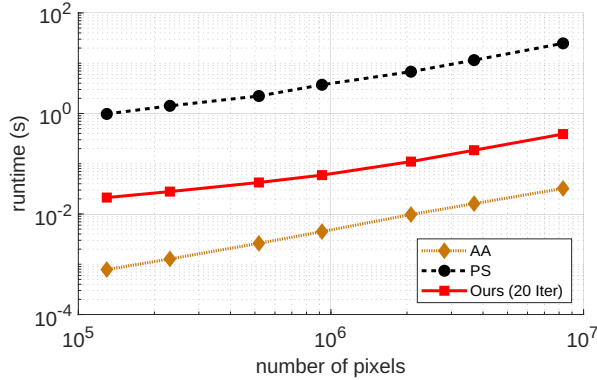


Figure 11: **Spatial Optimization Resolution Scaling Comparison.** Runtime depending on the image resolution for a 5% mask density. While the analytic approach is clearly the fastest, our method at least 50 times faster than PS for all image resolutions.

together with an adaptation to the local mask density with for example the Delaunay triangulation should be preferred over the probabilistic sparsification approach, as it significantly outperforms it in terms of quality as well as runtime.

**Resolution Runtime Scaling.** We also evaluate the spatial optimization methods over different image resolutions ranging from  $480 \times 270$  to  $3840 \times 2160$ . The results are shown in Figure 11.

While our Delaunay-based densification method is one order of magnitude slower than the qualitatively inferior analytic approach, it is at least 50 times faster than PS for all image resolution. As for the inpainting (see [49]), all spatial optimization methods also show a nearly linear behavior with respect to the number of image pixels in the double logarithmic plot. As the slope is approximately 1 for all methods, we observe an ideal linear scaling behavior.

*Visual Comparison.* A visual comparison of the different spatial optimization methods for a 5% mask density on the image *lofsdalen* is given in Figure 12. We observe that the analytic and to some extent also the neural approach lead to slightly blurrier edges compared to the other methods. While PS and PS+NLPE result in similarly sharp edges as our Delaunay densification, they can also lead to wrong colors in homogeneous areas, e.g. in the sky. This happens as PS generates too few mask-pixels in homogeneous areas, due to only considering pixel-wise errors.

**6.3. Tonal Optimization Experiments.** A visual example of tonal optimization is shown in Figure 13 for the 4K image *lofsdalen* with a 5% inpainting mask obtained with our Delaunay densification spatial optimization (see Figure 12). We can observe that the tonal optimization increases the overall contrast, which leads to an improvement of more than 1 dB.

*Voronoi Initialization.* Before we present results for the full tonal optimization framework, we evaluate the performance of our Voronoi initialization. Figure 14(a) shows a comparison with the iterated direct neighbor initialization based on [32]. For our Voronoi initialization we show results for two different weighting functions: a constant weighting and an inverse logarithmic distance weighting. We observe that all methods significantly improve the PSNR within a few iterations by around 1 dB. We can see that the PSNR starts to decrease after a few iterations, since we only solve a surrogate problem. Thus, it is necessary to stop the iteration once the PSNR begins to decrease and use the tonal values from the best iteration as the final result. Each iteration needs exactly one inpainting that takes around 15.4 ms, except for the very first iteration of the Voronoi approaches which needs to construct the Voronoi diagram, which takes around 8 ms. We can see that both Voronoi approaches outperform the direct neighbor approach by about 0.1 dB, while being 8 ms slower. The difference between the constant weighting and the inverse logarithmic distance weighting is, however, small. Since the weighting has no effect on the runtime, we choose the inverse logarithmic distance weighting. Overall, we can observe that the Voronoi diagram seems to be a better approximation of the mask pixel influence areas than a simple direct neighborhood.

In order to quantify the effect of our Voronoi approach on the tonal optimization problem, we perform an experiment using our RAS tonal optimization method with and without the Voronoi initialization. Additionally, we compare against a CGNR solver with the same multi-grid ORAS inpainting. Figure 14(b) shows the result for a 5% mask density. For a better visualization, we have omitted the results for the CGNR solver with CG inpainting, as each iteration needs approximately 0.8 seconds, which makes it clearly inferior to the other methods. We can observe that RAS converges significantly faster to the optimal PSNR compared to the CGNR method. When we use RAS together with the Voronoi initialization, we can stop the tonal optimization much earlier, even though the initial iteration takes longer. As the tonal optimization is a convex least squares problem, all tested methods eventually converge to the same optimal PSNR. Therefore, we omit a comparison of the reconstruction quality, as all methods end up with the same solution. The experiment also shows that the Voronoi initialization alone almost reaches the optimal PSNR up to 0.2 dB. **This proves that the Voronoi initialization is an essential tool for tonal optimization.**

*Runtime Scaling.* We evaluate our tonal optimization methods on multiple mask densities ranging from 0.5% up to 15%, which covers the density range for which homogeneous diffusion

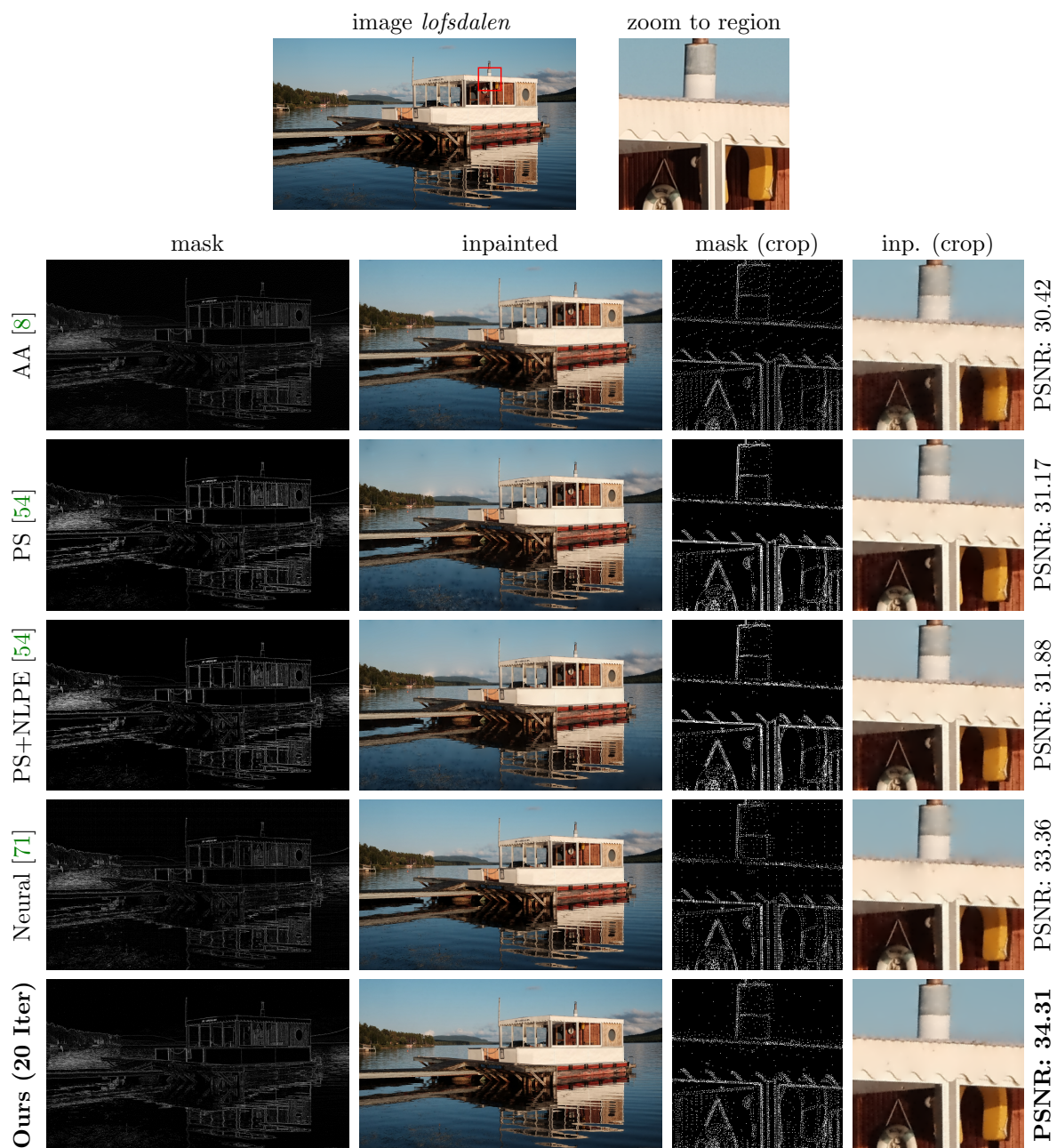


Figure 12: **Visual Comparison of Spatial Optimization for 5% Mask Density on Image *lofsdalen*.** PSNRs are for the whole image. Notice the blurry edges for the analytic approach and the discoloration present in the sky for PS and PS+NLPE.

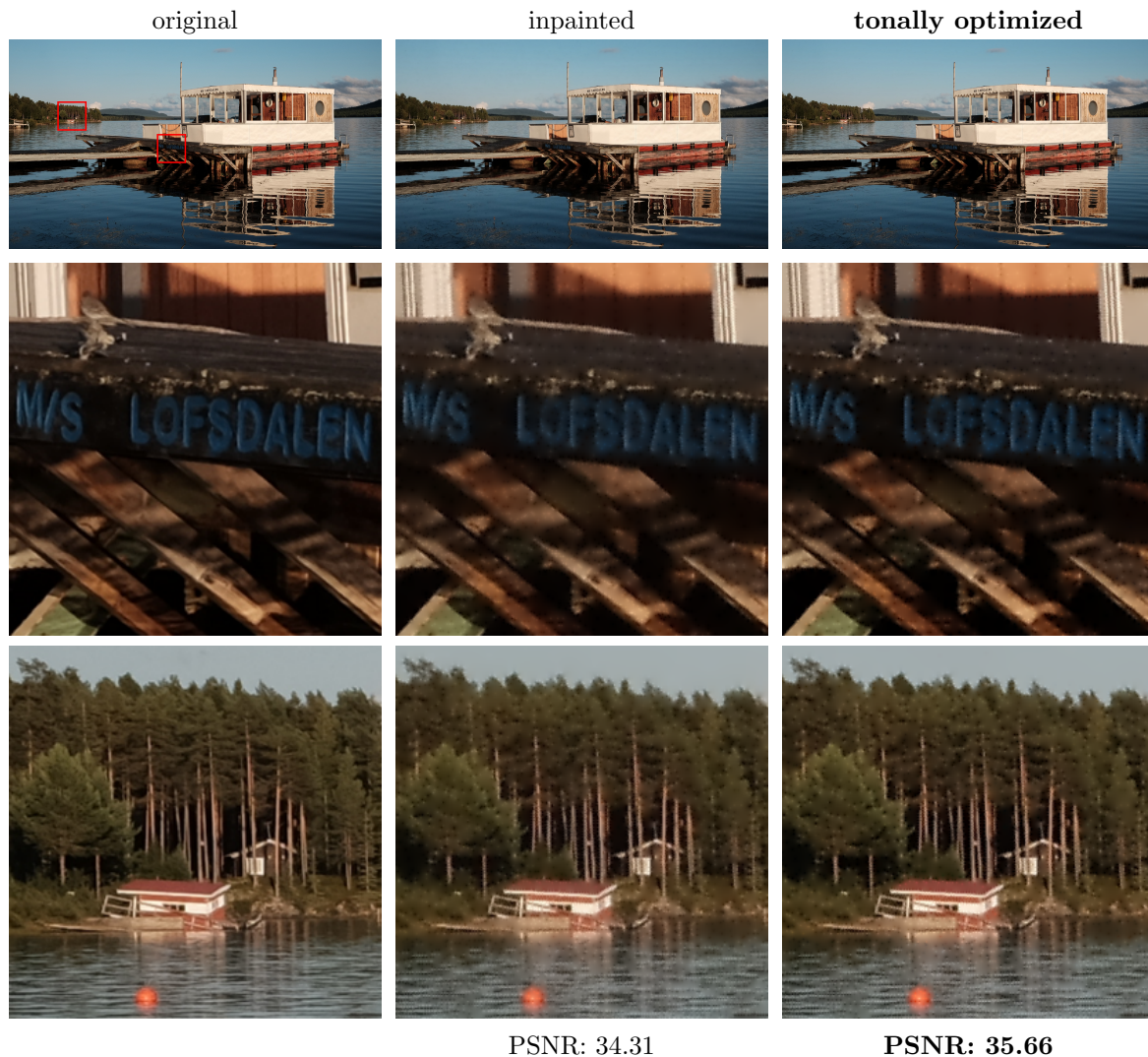


Figure 13: **Visual Comparison of Tonal Optimization for 5% Mask Density on Image *lofsdalen*.** PSNRs are for the whole image. Notice the enhanced contrast around the letters and the improved colors in the tonally optimized inpainting.

inpainting is practically relevant. As a stopping criterion for the tonal optimization, we use the relative improvement of the MSE. We stop when the MSE improves by less than 0.1%. The results are shown in Figure 15(a). We see that for all mask densities our RAS method with a Voronoi initialization outperforms CGNR with CG inpainting by more than one order of magnitude, and is clearly faster than CGNR with ORAS inpainting and the RAS method without the Voronoi initialization.

It also shows that all methods need more time for lower densities than for higher ones. This has two reasons: The runtime of the inpaintings within the tonal optimization depends on the mask density, as seen in [49]; but we also need fewer tonal optimization iterations the

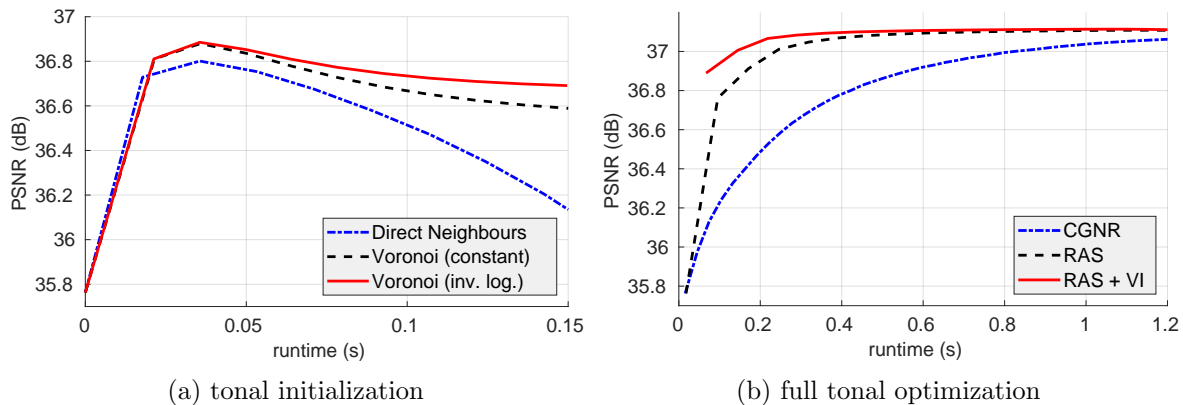


Figure 14: **Tonal Optimization Comparison for a 5% Mask Density.** (a) The Voronoi-based initialization approach clearly outperforms the neighbor-based approach. Using an inverse logarithmic weighting improves the quality slightly compared to a constant one. (b) Our RAS domain decomposition solver converges significantly faster than the simpler CGNR solver. Together with our Voronoi initialization (VI) RAS shows the best performance.

larger the density becomes, since the influence of pixels is more localized.

We also evaluate the tonal optimization methods over different image resolutions ranging from  $480 \times 270$  to  $3840 \times 2160$ . The results are shown in Figure 15(b). We see that for all image resolutions our RAS method with Voronoi initialization is at least one order of magnitude faster compared to CGNR with CG inpainting and around 60% faster than CGNR with ORAS multigrid inpainting. As for the inpainting (see [49]) and also the spatial optimization methods, all tonal optimization methods show a nearly linear behavior with respect to the number of image pixels in the double logarithmic plot with a slope of approximately 1. **This reveals that the tonal optimization problem has an underlying linear time complexity.**

**7. Conclusions and Outlook.** Inpainting-based compression does not only require a good inpainting method but also methods for the optimization of the inpainting data. The optimization of the spatial data as well as the tonal data for homogeneous diffusion inpainting is a challenging task, and previous approaches were either slow or of inferior quality. As a remedy, we developed new methods for the data optimization of homogeneous diffusion inpainting that outperform previous approaches by a wide margin. Furthermore, most prior approaches could handle only relatively small images, while we are able to work with images of 4K resolution and higher with optimal linear resolution to runtime scaling. We achieved this by carefully adapting some of the most successful numerical concepts and transferring them to an image compression application. For our spatial optimization method we combined a mask densification approach with error-map dithering ideas using a Delaunay triangulation. For the tonal optimization we adopted a domain decomposition method that solves the corresponding normal equations in a matrix-free fashion. Additionally we proposed a Voronoi-based initialization strategy that allows us to stop the tonal optimization much earlier. This allows us to create high quality inpainting masks and optimized tonal values in a runtime

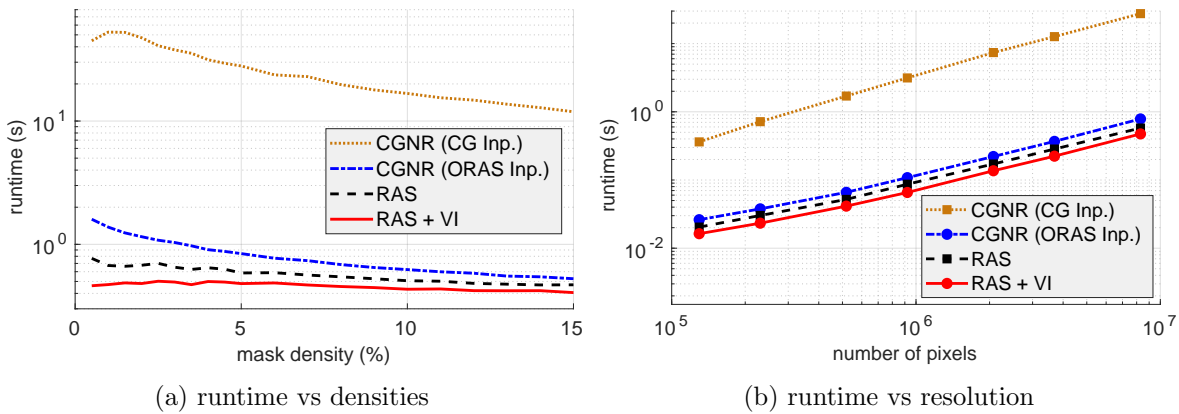


Figure 15: **Runtime Comparisons of the Tonal Optimization.** (a) Runtime depending on the mask density. Tonal optimization for lower mask densities takes longer for all methods without our Voronoi initialization (VI). RAS+VI is more than one order of magnitude faster compared to nested CG for all densities. (b) Runtime depending on the number of pixels (double logarithmic plot).

of less than a second on a contemporary GPU. This constitutes a significant improvement over any comparable previous approaches and suggests a similar order of runtime efficiency as JPEG2000, while solving a numerically much more challenging problem. We note, however, that the runtimes in our approach are for the data optimization and do not include an encoding step currently. Together with a real-time capable inpainting (see [49]), we presented a basis for inpainting-based compression methods that may serve as serious alternatives to classical transform-based codecs, both in terms of quality as well as runtimes.

So far we only considered the data optimization for homogeneous diffusion inpainting. However, many of our proposed methods can be extended to more sophisticated operators, such as anisotropic nonlinear diffusion that are able to qualitatively outperform homogeneous diffusion. Our Delaunay-based spatial optimization and our Voronoi-based initialization strategy for the tonal optimization are fairly general and can be used with most inpainting operators. In our ongoing research we investigate how well these methods perform with different inpainting operators and how they can be improved.

## REFERENCES

- [1] T. ACAR AND M. GÖKMEN, *Image coding using weak membrane model of images*, in Visual Communications and Image Processing '94, A. K. Katsaggelos, ed., vol. 2308 of Proceedings of SPIE, SPIE Press, Bellingham, 1994, pp. 1221–1230.
- [2] R. ACHANTA, N. ARVANITOPOULOS, AND S. SÜSTRUNK, *Extreme image completion*, in Proc. 42nd International Conference on Acoustics, Speech, and Signal Processing (ICASSP), New Orleans, USA, Mar. 2017, pp. 1333–1337.
- [3] M. D. ADAMS, *A highly-effective incremental/decremental delaunay mesh-generation strategy for image representation*, Signal Processing, 93 (2013), pp. 749–764.
- [4] T. ALT, P. PETER, AND J. WEICKERT, *Learning sparse masks for diffusion-based image inpainting*, in Pattern Recognition and Image Analysis, A. J. Pinho, P. Georgieva, L. F. Teixeira, and J. A. Sánchez, eds., vol. 13256 of Lecture Notes in Computer Science, Springer, Cham, 2022, pp. 528–539.

- [5] S. ANDRIS, P. PETER, R. M. KAJA MOHIDEEN, J. WEICKERT, AND S. HOFFMANN, *Inpainting-based video compression in FullHD*, in *Scale Space and Variational Methods in Computer Vision*, A. Elmoataz, J. Fadili, Y. Quéau, J. Rabin, and L. Simon, eds., vol. 12679 of *Lecture Notes in Computer Science*, Springer, Cham, 2021, pp. 425–436.
- [6] F. AURENHAMMER, R. KLEIN, AND D. LEE, *Voronoi Diagrams And Delaunay Triangulations*, World Scientific, Singapore, 2013.
- [7] V. BASTANI, M. HELFROUSH, AND K. KASIRI, *Image compression based on spatial redundancy removal and image inpainting*, *Journal of Zhejiang University – Science C (Computers & Electronics)*, 11 (2010), pp. 92–100.
- [8] Z. BELHACHMI, D. BUCUR, B. BURGETH, AND J. WEICKERT, *How to choose interpolation data in images*, *SIAM Journal on Applied Mathematics*, 70 (2009), pp. 333–352.
- [9] Z. BELHACHMI AND T. JACUMIN, *Iterative approach to image compression with noise: Optimizing spatial and tonal data*, 2022, <https://arxiv.org/abs/2209.14706>.
- [10] Z. BELHACHMI AND T. JACUMIN, *Optimal interpolation data for PDE-based compression of images with noise*, *Communications in Nonlinear Science and Numerical Simulation*, 109 (2022), Article 106278.
- [11] Z. BELHACHMI AND T. JACUMIN, *Adjoint method in PDE-based image compression*, 2023, <https://arxiv.org/abs/2302.02665>.
- [12] Å. BJÖRK, *Numerical Methods for Least Squares Problems*, SIAM, Philadelphia, 1996.
- [13] S. BONETTINI, I. LORIS, F. PORTA, M. PRATO, AND S. REBEGOLDI, *On the convergence of a linesearch based proximal-gradient method for nonconvex optimization*, *Inverse Problems*, 33 (2017), Article 055005.
- [14] F. BORNEMANN AND P. DEUFLHARD, *The cascadic multigrid method for elliptic problems*, *Numerische Mathematik*, 75 (1996), pp. 135–152.
- [15] A. BRANDT, *Multi-level adaptive solutions to boundary-value problems*, *Mathematics of Computation*, 31 (1977), pp. 333–390.
- [16] M. BREUSS, L. HOELTGEN, AND G. RADOW, *Towards PDE-based video compression with optimal masks prolonged by optic flow*, *Journal of Mathematical Imaging and Vision*, 63 (2021), pp. 144–156.
- [17] W. L. BRIGGS, V. E. HENSON, AND S. F. MCCORMICK, *A Multigrid Tutorial*, SIAM, Philadelphia, second ed., 2000.
- [18] X.-C. CAI AND M. SARKIS, *A restricted additive Schwarz preconditioner for general sparse linear systems*, *SIAM Journal on Scientific Computing*, 21 (1999), pp. 792–797.
- [19] S. CARLSSON, *Sketch based coding of grey level images*, *Signal Processing*, 15 (1988), pp. 57–83.
- [20] Y. CHEN, R. RANFTL, AND T. POCK, *A bi-level view of inpainting-based image compression*, in *Proc. 19th Computer Vision Winter Workshop*, Z. Kúkelová and J. Heller, eds., Křtiny, Czech Republic, Feb. 2014, pp. 19–25.
- [21] V. CHIZHOV AND J. WEICKERT, *Efficient data optimisation for harmonic inpainting with finite elements*, in *Computer Analysis of Images and Patterns*, N. Tsapatsoulis, A. Panayides, T. Theo, A. Lanitis, C. Pattichis, and M. Vento, eds., vol. 13053 of *Lecture Notes in Computer Science*, Springer, Cham, 2021, pp. 432–441.
- [22] Q. DAI, H. CHOPP, E. POUYET, O. COSSAIRT, M. WALTON, AND A. K. KATSAGGELOS, *Adaptive image sampling using deep learning and its application on X-ray fluorescence image reconstruction*, *IEEE Transactions on Multimedia*, 22 (2020), pp. 2564–2578.
- [23] V. DAROPOULOS, M. AUGUSTIN, AND J. WEICKERT, *Sparse inpainting with smoothed particle hydrodynamics*, *SIAM Journal on Imaging Sciences*, 14 (2021), pp. 1669–1704.
- [24] L. DEMARET, N. DYN, AND A. ISKE, *Image compression by linear splines over adaptive triangulations*, *Signal Processing*, 86 (2006), pp. 1604–1616.
- [25] U. Y. DESAI, M. M. MIZUKI, I. MASAKI, AND B. K. P. HORN, *Edge and mean based image compression*, Tech. Report 1584 (A.I. Memo), Artificial Intelligence Lab., Massachusetts Institute of Technology, Cambridge, MA, Nov. 1996.
- [26] M. DI MARTINO AND G. FACCIOLO, *An analysis and implementation of multigrid Poisson solvers with verified linear complexity*, *Image Processing On Line*, 8 (2018), pp. 192–218.
- [27] R. DISTASI, M. NAPPI, AND S. VITULANO, *Image compression by B-tree triangular coding*, *IEEE Transactions on Communications*, 45 (1997), pp. 1095–1100.
- [28] V. DOLEAN, P. JOLIVET, AND F. NATAF, *An Introduction to Domain Decomposition Methods: Algo-*

- rithms, Theory, and Parallel Implementation*, SIAM, Philadelphia, 2015.
- [29] E. EFSTATHIOU AND M. J. GANDER, *Why restricted additive Schwarz converges faster than additive Schwarz*, BIT Numerical Mathematics, 43 (2003), pp. 945–959.
- [30] B. E. EL MARZOUKI AND M. D. ADAMS, *An improved incremental/decremental delaunay mesh-generation strategy for image representation*, in 2017 IEEE Pacific Rim Conference on Communications, Computers and Signal Processing (PACRIM), Victoria, Canada, Aug. 2017, pp. 1–6.
- [31] R. W. FLOYD AND L. STEINBERG, *An adaptive algorithm for spatial grey scale*, Proceedings of the Society of Information Display, 17 (1976), pp. 75–77.
- [32] I. GALIĆ, J. WEICKERT, M. WELK, A. BRUHN, A. BELYAEV, AND H.-P. SEIDEL, *Image compression with anisotropic diffusion*, Journal of Mathematical Imaging and Vision, 31 (2008), pp. 255–269.
- [33] M. J. GANDER, *Schwarz methods over the course of time*, Electronic Transactions on Numerical Analysis, 31 (2008), pp. 228–255.
- [34] J. GAUTIER, O. LE MEUR, AND C. GUILLEMOT, *Efficient depth map compression based on lossless edge coding and diffusion*, in Proc. 2012 Picture Coding Symposium, Kraków, Poland, May 2012, pp. 81–84.
- [35] C. GUILLEMOT AND O. LE MEUR, *Image inpainting: Overview and recent advances*, IEEE Signal Processing Magazine, 31 (2014), pp. 127–144.
- [36] W. HACKBUSCH, *Multigrid Methods and Applications*, Springer, New York, 1985.
- [37] M. HESTENES AND E. STIEFEL, *Method of conjugate gradients for solving linear systems*, Journal of Research of the National Bureau of Standards, 49 (1951), pp. 409–438.
- [38] N. J. HIGHAM, *Accuracy and Stability of Numerical Algorithms*, SIAM, Philadelphia, second ed., 2002.
- [39] L. HOELTGEN, S. SETZER, AND J. WEICKERT, *An optimal control approach to find sparse data for Laplace interpolation*, in Energy Minimisation Methods in Computer Vision and Pattern Recognition, A. Heyden, F. Kahl, C. Olsson, M. Oskarsson, and X.-C. Tai, eds., vol. 8081 of Lecture Notes in Computer Science, Springer, Berlin, 2013, pp. 151–164.
- [40] L. HOELTGEN AND J. WEICKERT, *Why does non-binary mask optimisation work for diffusion-based image compression?*, in Energy Minimisation Methods in Computer Vision and Pattern Recognition, X.-C. Tai, E. Bae, T. F. Chan, S. Y. Leung, and M. Lysaker, eds., vol. 8932 of Lecture Notes in Computer Science, Springer, Berlin, 2015, pp. 85–98.
- [41] S. HOFFMANN, *Competitive Image Compression with Linear PDEs*, PhD thesis, Department of Computer Science, Saarland University, Saarbrücken, Germany, 2017.
- [42] S. HOFFMANN, M. MAINBERGER, J. WEICKERT, AND M. PUHL, *Compression of depth maps with segment-based homogeneous diffusion*, in Scale Space and Variational Methods in Computer Vision, A. Kuijper, K. Bredies, T. Pock, and H. Bischof, eds., vol. 7893 of Lecture Notes in Computer Science, Springer, Berlin, 2013, pp. 319–330.
- [43] S. HOFFMANN, G. PLONKA, AND J. WEICKERT, *Discrete Green’s functions for harmonic and biharmonic inpainting with sparse atoms*, in Energy Minimization Methods in Computer Vision and Pattern Recognition, X.-C. Tai, E. Bae, T. F. Chan, and M. Lysaker, eds., vol. 8932 of Lecture Notes in Computer Science, Springer, Berlin, 2015, pp. 169–182.
- [44] T. IJIMA, *Basic theory on normalization of pattern (in case of typical one-dimensional pattern)*, Bulletin of the Electrotechnical Laboratory, 26 (1962), pp. 368–388. In Japanese.
- [45] F. JOST, V. CHIZHOV, AND J. WEICKERT, *Optimising different feature types for inpainting-based image representations*, in Proc. 48th International Conference on Acoustics, Speech, and Signal Processing (ICASSP), Rhodes, Greece, June 2023, IEEE Computer Society Press.
- [46] F. JOST, P. PETER, AND J. WEICKERT, *Compressing piecewise smooth images with the Mumford-Shah cartoon model*, in Proc. 28th European Signal Processing Conference (EUSIPCO), Amsterdam, Netherlands, Jan. 2021, pp. 511–515.
- [47] I. JUMAKULYYEV AND T. SCHULTZ, *Combining image space and q-space PDEs for lossless compression of diffusion MR images*, Journal of Mathematical Imaging and Vision, 65 (2023), pp. 644–656.
- [48] E. KALMOUN AND M. NASSER, *Harmonic image inpainting using the charge simulation method*, Pattern Analysis and Applications, 25 (2022), pp. 795–806.
- [49] N. KÄMPER, V. CHIZHOV, AND J. WEICKERT, *Multigrid domain decomposition for real-time homogeneous diffusion inpainting in 4K*, Aug. 2024, <https://arxiv.org/abs/2401.06744>.
- [50] L. KAROS, P. BHEED, P. PETER, AND J. WEICKERT, *Optimising data for exemplar-based inpaint-*



- ing*, in *Advanced Concepts for Intelligent Vision Systems*, J. Blanc-Talon, D. Helbert, W. Philips, D. Popescu, and P. Scheunders, eds., vol. 11182 of *Lecture Notes in Computer Science*, Springer, Berlin, 2018, pp. 547–558.
- [51] Y. LI, M. SJOSTROM, U. JENNEHAG, AND R. OLSSON, *A scalable coding approach for high quality depth image compression*, in *Proc. 3DTV-Conference: The True Vision – Capture, Transmission and Display of 3D Video*, Zurich, Switzerland, Oct. 2012.
- [52] D. LIU, X. SUN, F. WU, S. LI, AND Y.-Q. ZHANG, *Image compression with edge-based inpainting*, *IEEE Transactions on Circuits, Systems and Video Technology*, 17 (2007), pp. 1273–1286.
- [53] M. MAINBERGER, A. BRUHN, J. WEICKERT, AND S. FORCHHAMMER, *Edge-based compression of cartoon-like images with homogeneous diffusion*, *Pattern Recognition*, 44 (2011), pp. 1859–1873.
- [54] M. MAINBERGER, S. HOFFMANN, J. WEICKERT, C. H. TANG, D. JOHANNSEN, F. NEUMANN, AND B. DOERR, *Optimising spatial and tonal data for homogeneous diffusion inpainting*, in *Scale Space and Variational Methods in Computer Vision*, A. M. Bruckstein, B. ter Haar Romeny, A. M. Bronstein, and M. M. Bronstein, eds., vol. 6667 of *Lecture Notes in Computer Science*, Springer, Berlin, 2012, pp. 26–37.
- [55] D. MARWOOD, P. MASSIMINO, M. COVELL, AND S. BALUJA, *Representing images in 200 bytes: Compression via triangulation*, in *Proc. 2018 IEEE International Conference on Image Processing (ICIP)*, Athens, Greece, Oct. 2018, pp. 405–409.
- [56] Y. MELNIKOV AND M. MELNIKOV, *Computability of series representations for Green’s functions in a rectangle*, *Engineering Analysis with Boundary Elements*, 30 (2006), pp. 774–780.
- [57] P. OCHS, Y. CHEN, T. BROX, AND T. POCK, *iPiano: Inertial proximal algorithm for nonconvex optimization*, *SIAM Journal on Imaging Sciences*, 7 (2014), pp. 1388–1419.
- [58] C. C. PAIGE AND M. A. SAUNDERS, *Solution of sparse indefinite systems of linear equations*, *SIAM Journal on Numerical Analysis*, 12 (1975), pp. 617–629.
- [59] W. B. PENNEBAKER AND J. L. MITCHELL, *JPEG: Still Image Data Compression Standard*, Springer, New York, 1992.
- [60] P. PETER, *Fast inpainting-based compression: Combining Shepard interpolation with joint inpainting and prediction*, in *Proc. 2019 IEEE International Conference on Image Processing (ICIP)*, Taipei, Taiwan, Sept. 2019, pp. 3557–3561.
- [61] P. PETER, *A Wasserstein GAN for joint learning of inpainting and its spatial optimisation*, in *Image and Video Technology*, H. Wang, W. Lin, P. Manoranjan, G. Xiao, K. Chan, X. Wang, G. Ping, and H. Jiang, eds., vol. 13763 of *Lecture Notes in Computer Science*, Springer, Cham, 2023, pp. 132–145.
- [62] P. PETER, S. HOFFMANN, F. NEDWED, L. HOELTGEN, AND J. WEICKERT, *Evaluating the true potential of diffusion-based inpainting in a compression context*, *Signal Processing: Image Communication*, 46 (2016), pp. 40–53.
- [63] P. PETER, C. SCHMALTZ, N. MACH, M. MAINBERGER, AND J. WEICKERT, *Beyond pure quality: Progressive mode, region of interest coding and real time video decoding in PDE-based image compression*, *Journal of Visual Communication and Image Representation*, 31 (2015), pp. 256–265.
- [64] P. PETER, K. SCHRADER, T. ALT, AND J. WEICKERT, *Deep spatial and tonal data optimisation for homogeneous diffusion inpainting*, To Appear in *Pattern Analysis and Applications*, (2023).
- [65] G. PLONKA, S. HOFFMANN, AND J. WEICKERT, *Pseudo-inverses of difference matrices and their application to sparse signal approximation*, *Linear Algebra and its Applications*, 503 (2016), pp. 26–47.
- [66] K. R. RAO AND P. YIP, *Discrete Cosine Transform: Algorithms, Advantages, Applications*, Academic Press Professional, Inc., San Diego, CA, USA, 1990.
- [67] J. RASCH, J. PFAFF, M. SCHÄFER, A. HENKEL, H. SCHWARZ, D. MARPE, AND T. WIEGAND, *A signal adaptive diffusion filter for video coding: Mathematical framework and complexity reductions*, *Signal Processing: Image Communication*, 85 (2020), Article 115861.
- [68] G. RONG AND T.-S. TAN, *Jump flooding in GPU with applications to Voronoi diagram and distance transform*, in *Proceedings of the 2006 Symposium on Interactive 3D Graphics and Games, I3D ’06*, New York, NY, USA, 2006, Association for Computing Machinery, pp. 109–116.
- [69] Y. SAAD, *Iterative Methods for Sparse Linear Systems*, SIAM, Philadelphia, second ed., 2003.
- [70] C. SCHMALTZ, P. PETER, M. MAINBERGER, F. EBEL, J. WEICKERT, AND A. BRUHN, *Understanding, optimising, and extending data compression with anisotropic diffusion*, *International Journal of Computer Vision*, 108 (2014), pp. 222–240.

- [71] K. SCHRADER, P. PETER, N. KÄMPER, AND J. WEICKERT, *Efficient neural generation of 4K masks for homogeneous diffusion inpainting*, in Scale Space and Variational Methods in Computer Vision, L. Calatroni, M. Donatelli, S. Morigi, M. Prato, and M. Santavesaria, eds., vol. 14009 of Lecture Notes in Computer Science, Springer, Cham, 2023, pp. 16–28.
- [72] T. SCHÜTZE AND H. SCHWETLICK, *Bivariate free knot splines*, BIT Numerical Mathematics, 43 (2003), pp. 153–178.
- [73] A. SOLÉ, V. CASELLES, G. SAPIRO, AND F. ARANDIGA, *Morse description and geometric encoding of digital elevation maps*, IEEE Transactions on Image Processing, 13 (2004), pp. 1245–1262.
- [74] A. ST-CYR, M. J. GANDER, AND S. J. THOMAS, *Optimized multiplicative, additive, and restricted additive Schwarz preconditioning*, SIAM Journal on Scientific Computing, 29 (2007), pp. 2402–2425.
- [75] G. STRANG, *The discrete cosine transform*, SIAM Review, 41 (1999), pp. 135–147.
- [76] G. J. SULLIVAN, J.-R. OHM, W.-J. HAN, AND T. WIEGAND, *Overview of the high efficiency video coding (HEVC) standard*, IEEE Transactions on Circuits, Systems and Video Technology, 22 (2012), pp. 1649–1668.
- [77] D. S. TAUBMAN AND M. W. MARCELLIN, *JPEG 2000: Image Compression Fundamentals, Standards and Practice*, Kluwer, Boston, 2002.
- [78] A. TOSELLI AND O. WIDLUND, *Domain Decomposition Methods - Algorithms and Theory*, vol. 34 of Springer Series in Computational Mathematics, Springer, Berlin, Heidelberg, 2005.
- [79] U. TROTTEBERG, C. OOSTERLEE, AND A. SCHÜLLER, *Multigrid*, Academic Press, San Diego, 2001.
- [80] D. TSCHUMPERLÉ, C. PORQUET, AND A. MAHBOUBI, *Reconstruction of smooth 3d color functions from keypoints: Application to lossy compression and exemplar-based generation of color luts*, SIAM Journal on Imaging Sciences, 13 (2020), pp. 1511–1535.
- [81] J. WEICKERT, *Anisotropic Diffusion in Image Processing*, Teubner, Stuttgart, 1998.
- [82] H. WENDLAND, *Scattered Data Approximation*, Cambridge University Press, Cambridge, UK, 2010.
- [83] P. WESSELING, *An Introduction to Multigrid Methods*, R. T. Edwards, Flourtown, 2004.
- [84] Y. WU, H. ZHANG, Y. SUN, AND H. GUO, *Two image compression schemes based on image inpainting*, in Proc. 2009 International Joint Conference on Computational Sciences and Optimization, Sanya, China, Apr. 2009, IEEE Computer Society Press, pp. 816–820.
- [85] Z. XIONG, X. SUN, AND F. WU, *Block-based image compression with parameter-assistant inpainting*, IEEE Transactions on Image Processing, 19 (2010), pp. 1651–1657.
- [86] C. ZHAO AND M. DU, *Image compression based on PDEs*, in Proc. 2011 International Conference of Computer Science and Network Technology, Harbin, China, Dec. 2011, pp. 1768–1771.